

DISTANCES, METALLICITIES, AND AGES OF DWARF ELLIPTICAL GALAXIES IN THE VIRGO CLUSTER FROM SURFACE BRIGHTNESS FLUCTUATIONS

H. JERJEN

Research School of Astronomy and Astrophysics, The Australian National University, Mt Stromlo Observatory, Cotter Road, Weston ACT 2611, Australia

B. BINGGELI AND F.D. BARAZZA

Astronomical Institute of the University of Basel, Venusstrasse 7, CH-4102 Binningen, Switzerland

Accepted for publication in the Astronomical Journal

ABSTRACT

We have employed FORS1 and 2 at the Very Large Telescope at ESO to acquire deep B and R -band CCD images of 16 dwarf elliptical galaxies in the direction of the Virgo cluster. For each dwarf we measure the apparent R -band surface brightness fluctuation (SBF) magnitude \bar{m}_R and the $(B-R)_0$ colour in a number of fields at different galactocentric distances. From the field-to-field variation of the two quantities we determine the SBF distance by means of the $(B-R)_0 - \bar{M}_R$ relation. The derived distances of the dwarfs are ranging from 14.9 Mpc to 21.3 Mpc, with a mean 1σ uncertainty of 1.4 Mpc or 8% of the distance, confirming that there is considerable depth in the distance distribution of early-type cluster members. For VCC1104 (IC3388) our SBF distance modulus of $(m-M)_{\text{SBF}} = 31.15 \pm 0.19$ (17.0 \pm 1.5 Mpc) is in good agreement with the Harris et al. (1998) result of $(m-M)_{\text{TRGB}} = 30.98 \pm 0.19$ mag (15.7 \pm 1.5 Mpc) based on HST observations and the tip magnitude of the red giant branch. Combining our results with existing distances for giant Virgo ellipticals we identify two major galaxy concentrations in the distance distribution: a broad primary clump around $(M-m) = 31.0$ mag (15.8 Mpc) and a narrow secondary clump around 31.33 mag (18.5 Mpc). An adaptive kernel analysis finds the two concentrations to be significant at the 99% (2.5σ) and 89% (1.6σ) levels. While the near-side clump of Virgo early-type galaxies can be associated to the subcluster centered on M87, the second clump is believed to be mainly due to the backside infalling group of galaxies around M86.

The ages and metallicities of the dE stellar populations are estimated by combining the observed $(B-R)_0$ colours with Worthey's stellar population synthesis models. It appears that the Virgo dEs cover a wider range in metallicity, from $[\text{Fe}/\text{H}] \approx -1.4$ (VCC0815) to -0.5 (NGC4415), than Fornax cluster dEs. The derived metallicities place the Virgo dEs on the extension of the metallicity–luminosity relation defined by the low-luminosity Local Group dEs. The data further suggest an age range from genuinely old (~ 17 Gyrs) stellar systems like IC3019 and IC0783 to intermediate-age (8–12 Gyrs) dwarfs like NGC4431 and IC3468.

Subject headings: galaxies: clusters: individual (Virgo) – galaxies: distances and redshifts – galaxies: dwarf – galaxies: elliptical and lenticular, cD – galaxies: individual (IC3328, IC3388) – galaxies: stellar content

1. INTRODUCTION

The nearby Virgo Cluster is a largely extended and complex structure of over 1300 galaxies and represents the major feature of the Local Supercluster. Based on the pioneering work by de Vaucouleurs (1961), the photographic Las Campanas survey by Binggeli et al. (1985, hereafter the Virgo Cluster Catalog or VCC) and a complementary collection of galaxy redshifts (Binggeli et al. 1993), a number of subclumps and gravitationally unbound clouds were identified in Virgo from imaging and recessional velocity data. Centrally located are two separate subclumps each dominated by a giant elliptical galaxy, i.e. M87 and M86 (see Binggeli 1999). On a large scale there is another structure along the north-south axis of the Virgo cluster, defined by the northern M87/M86 subclumps (called “cluster A” in Binggeli et al. 1987) and the southern galaxy concentration around M49, called here the “M49 subclump” (= “cluster B”). These subclusters are bound to the south and west by three galaxy clouds named W, W’ (de Vaucouleurs 1961), and M (Ftaclas et al. 1984).

The knowledge of a precise distance to the Virgo cluster or more generally a good understanding of its three dimen-

sional structure plays an important role in many research areas of extragalactic astronomy. However, despite the large effort to resolve these issues over the past decades, the spatial extension of the Virgo cluster remained highly uncertain. The reasons are twofold. Firstly, only a relative small number of cluster member galaxies had accurate distance measurements. Secondly, the typical target objects were spiral galaxies which reside, according to the morphology–density relation (Dressler 1980), in the outskirts of galaxy clusters. So it should come as no surprise that using accurate distance indicators like Cepheids and Supernovae of type Ia revealed a significant distance spread among the Virgo spirals ranging from 15 Mpc (eg. Graham et al. 1999; Saha et al. 2001) to 25 Mpc (eg. Saha et al. 1997). These heavily disputed results simply reflect the line-of-sight depth of the large spiral halo of the Virgo cluster and demonstrated why accurate distance measurements of only a few spirals are of limited use.

Progress towards a precise mapping of the 3D-structure of the Virgo cluster region was made only when the numbers of spiral galaxy distances were increased (e.g. Yasuda et al. 1997). Alternatively, fundamental plane distance measurements (Gavazzi et al. 1999) and surface brightness fluctuations (Neilsen & Tsvetanov 2000; Tonry et al. 2001) were employed to locate the more centrally concentrated early-type

giant elliptical galaxies. Similar to the giant brethren, the less luminous and more elusive dwarf elliptical (dE) galaxies are well confined to the highest galaxy densities in a cluster (the morphology–density relation for dwarfs, Binggeli et al. 1987). But it is their occurrence in large numbers in cluster cores (Binggeli et al. 1985; Ferguson & Binggeli 1994; Jerjen & Dressler 1997) that makes them unique and even more valuable than giant ellipticals. Dwarf ellipticals are the only galaxy type that flag the gravitational center(s) in a galaxy cluster *and* are available in statistically sufficient numbers.

Despite the great potential dEs offer to examine the densest regions of galaxy clusters only little work has been done with dEs to date due to the lack of an accurate and practical distance indicator. Correlations between global parameters of dEs such as the effective surface brightness–luminosity relation (Binggeli & Cameron 1991) or the shape parameter–luminosity relation (Jerjen & Binggeli 1997; Binggeli & Jerjen 1998) have considerable scatter and thus are not reliable to measure individual distances. Instead, the resolution power of the HST has to be used to resolve the stellar populations of dEs to establish distances by means of the tip magnitude of the red giant branch (TRGB, e.g. Karachentsev et al. 2000). While this approach works well for nearby dEs it becomes exceedingly difficult (crowding effects) and expensive (long integration times) to obtain good S/N stellar photometry at the required limiting magnitude with larger distances. This explains why the TRGB method was applied to only one dE (VCC1104 or IC3388) in the Virgo cluster (Harris et al. 1998) to date.

Considering the limitation of the TRGB method, another distance indicator has emerged as a substitute for measuring accurate distances to dEs beyond 10 Mpc from the Local Group. This is the surface brightness fluctuation method based on the discrete sampling of an *unresolved* stellar population in a galaxy with a CCD detector and the resulting Poisson fluctuations in the number of stars within a resolution element (Tonry & Schneider 1988). The method has been extensively tested in the Sculptor Group (Jerjen et al. 1998), Centaurus A group (Jerjen et al. 2000), M81 Group, the Canes Venatici cloud and the near field (Jerjen et al. 2001). First results from dwarf ellipticals in the more distant Fornax cluster (Jerjen 2003) and Centaurus cluster (Mieske et al. 2003) were reported recently. The high accuracy of the method (10–20%) opens up the possibility to measure precise distances to cluster dEs in a simple and efficient way.

The goal of this paper is threefold. First, we will measure the Surface Brightness Fluctuation distances of a sample of 16 dwarf elliptical galaxies in the direction of the Virgo cluster. We introduce the dwarf galaxies with their basic properties in §2. In §3 we describe the observations and data reduction. In §4 we will carry out the SBF analysis and calculate the fluctuation signals. We determine the SBF distances of the sample galaxies in §5. Second, we will investigate the distance distribution of the dwarfs in the context of the 3D-structure of the cluster in §6. Lastly, we will estimate rough metallicities and ages for our early-type galaxies in §7 using the fluctuation magnitudes and B-R broadband colour. Our conclusions are given in §8.

2. FUNDAMENTAL PROPERTIES OF THE SAMPLE

To follow-up the question on the 3D-distribution of the dE population in the Virgo cluster and to search for the gravitational centre(s) of the cluster, we have studied a sample of 16 early-type dwarfs from the Virgo Cluster Cata-

log (VCC; Binggeli et al. 1985). As it is a main requirement for the successful application of the SBF method, galaxies were primarily selected on their morphological appearance, i.e. type “dE(N)” or “dS0(N)” and on their apparent size, i.e. an isophotal radius $r_{B,25} > 30''$ and small ellipticity. Within these constraints, dwarfs were chosen in a way to get a good coverage in velocity space ($-730 \text{ km s}^{-1} < V_{\odot} < 1850 \text{ km s}^{-1}$) and in the celestial distribution ($12^{\text{h}}05^{\text{m}} < \text{R.A.}(1950) < 12^{\text{h}}40^{\text{m}}$; $+08^{\circ}00' < \text{Decl.}(2000) < +16^{\circ}30'$). A few dwarfs like VCC0810 simply came into our sample because they were close neighbours of our target galaxy. Finally, we added the nucleated dE galaxy VCC1104 (IC3388) to the sample. VCC1104 is the only Virgo dE for which an independent distance measurement is available (Harris et al. 1998).

Fig. 1 shows the galaxy distribution in the central region of the Virgo cluster with our sample galaxies highlighted as filled circles. In projection, all except two dwarfs are located in cluster A (M87/M86 subclump). VCC0929 (NGC4415) and VCC0856 (IC3328) are both cluster B objects. In Table 1 we list the fundamental parameters of our dwarfs. The VCC numbers (col. [1]), other names (col. [2]), and the morphological types (col. [3]) were taken from Binggeli et al. (1985). The J2000 coordinates are given in cols.[4-5] and the cluster region where the galaxy is found in col. [6]. The total *B* magnitudes (col. [7]) are taken from Barazza et al. (2003) and the heliocentric velocities (col. [8]) are from Binggeli et al. (1985, 1993) and Conselice et al. (2001).

A full account of the photometric properties of the galaxies based on new CCD data, including a comprehensive discussion of the characteristics of the surface brightness profiles, colour gradients, and structure parameters, is given elsewhere (Barazza et al. 2003). We note that the dEs have total absolute *B* luminosities in the range $-17.5 < M_{B_T} < -14.5$ and thus are at the bright end of the type-specific luminosity function for dEs (Sandage et al. 1985; Jerjen & Tammann 1997). As such these systems are typical cluster dEs with no counterparts known in low density environments i.e. galaxy groups or in the field as satellite galaxies. Only four of our dEs are fainter than the M31 companion NGC 205 ($M_{B_T} = -15.6$), a dE that is among the brightest early-type dwarfs found outside of clusters.

3. OBSERVATIONS

3.1. Data acquisition and reduction

Deep CCD images of the Virgo dEs have been acquired in the *B* and *R* passbands in service mode using the two first units of the Very Large Telescope at ESO Paranal Observatory over a period of two semesters: at UT1+FORs1 during an observing run on July 10–14, 1999 and at UT2+FORs2 during dark time periods in March–May, 2000. The detectors of the FORs (FOcal Reducer/Low dispersion Spectrograph) instruments are thinned and anti-reflection coated Tektronix (FORs1) and SiTE (FORs2) CCDs with 2048×2048 pixels. By default, service observations were taken in standard resolution mode, with a high gain and a pixel scale of $0''.2 \text{ pixel}^{-1}$ that yields a field of view of $6'.8 \times 6'.8$. The CCDs were read out in the four-port mode, i.e. four amplifiers read out one quarter of the CCD each. Target galaxies were positioned close to the center of one of the four quadrants leaving the other three “empty” and thus useful as night flats. Three exposures of 400–600 sec durations with slightly different pointings were secured in each filter for each galaxy. The Bessell *R* broadband filter was used at UT1+FORs1 while Bessell *B*

and R_s filters were employed at UT2+FORs2. Table 2 summarises the log of the observations.

Template bias frames were subtracted from all CCD images. Twilight sky exposures were median-averaged after level normalisation to obtain twilight masterflats. Flatfielding with the masterflats did produce no satisfactory results in all cases and reliable nightflats, which might have worked better, were unfortunately impossible to construct from the science frames. To remove the background gradients noticeable in some of the images, above all in the R (or R_s) frames, we fitted instead third-order polynomials to the sky background (see Barazza et al. 2003 for more details). The systematic uncertainty in the residual images due to this sky flattening problem was measured less than 0.1% over the full CCD area in all passbands, with the random errors being much smaller.

3.2. Photometric Calibration

All CCD data were acquired on nights with photometric sky quality. In service mode, a series of Landolt (1992) photometric standard stars are observed in various passbands under different airmasses every night. Fields which contained saturated standard stars when using short exposure times (~ 1 sec) were reobserved in the low gain mode. The analysis of fields taken in both gain modes confirmed the inverse gain ratios for the four CCD quadrants given in the FORs1+2 User Manual Issue 2.1 of ESO. Finally, we scaled the low gain frames to match the high gain images. In that way, photometric data over a larger magnitude range became available. From each series of standard stars observations we computed photometric zero points, extinction coefficients and color terms using the IRAF¹ package. For the observing period 65 the extinction coefficients and color terms could be compared with the values reported by the VLT Quality Control and Trending Services (Hanuschik & Silva 2002²) finding good agreement:

$$\text{ESO: } k_B = 0.25, \quad k_R = 0.09, \quad c_{(B-R)} = -0.08$$

$$\text{Our study: } k_B = 0.24, \quad k_R = 0.09, \quad c_{(B-R)} = -0.07$$

The photometric zero points varied significantly over the observing period 65. Therefore, we used the photometric zero points we determined for each observing night from our own set of standard stars. Formal photometric accuracies in the different passbands are 0.03 mag (Bessell B), 0.02 mag (Bessell R), and 0.02 mag (R_s). QC information for the observing period 63 was not available.

All images of a galaxy were registered by matching the positions of ≈ 100 reference stars on each CCD frame using *starfind*, *xyxymatch* and *imalign*. The sky-subtracted images taken in the same passband were cleaned from cosmic rays with *crreject* and co-added with *imcombine*. Finally, The resulting master images were flux calibrated.

4. SBF ANALYSIS

The R -band galaxy images were prepared for the SBF analysis following the recipes of Jerjen et al. (2000; 2001). This includes

- using DAOPHOT II (Stetson 1987) to clean the images from foreground stars, globular clusters, and back-

¹ IRAF is distributed by the National Optical Astronomy Observatories, which is operated by the Association of Universities for Research in Astronomy, Inc., under contract with the National Science Foundation

² see also http://www.eso.org/observing/dfo/quality/FORS/trend_query_form.html

ground galaxies brighter than magnitude $m_c = 27.0$ mag (≈ 500 ADUs in R and 600 ADUs in R_s).

- modeling the 2-dimensional galaxy surface brightness distribution.
- subtracting the best-fitting galaxy model from the master image.
- noise normalization of the residual image.

Between three and seven square subimages (hereafter SBF fields) were then defined on a fluctuation image within the $25.5 R$ mag arcsec⁻² isophotal limit thereby avoiding areas with previously identified disturbing sources or non-radial irregular features such as dust or spiral features (Jerjen et al. 2000; Jerjen et al. 2001; Barazza et al. 2002). The size of the SBF fields was chosen between 60×60 and 120×120 pixels depending on the apparent size of the galaxy. Assuming an average seeing of 0.6 arcsec (see Table 2), a field carries the SBF signal from 400 to 1600 independent points. In total we defined 80 SBF fields in our 16 sample galaxies.

The SBF fields were Fourier transformed and the azimuthally averaged power spectra calculated. From isolated bright stars on the master image we determined the point spread function (PSF) profile. We then fitted a linear combination of the flux normalized and exposure time weighted PSF power spectrum and a constant at the observed galaxy power spectrum $PS(k) = P_0 PS_{\text{star}}(k) + P_1$, demanding a least-squares minimisation. Data points at low spatial frequencies ($k \leq 5$) were omitted as they are likely affected by imperfect galaxy model subtraction. Figs. 2 and 3 show the power spectrum of each SBF field with the best fitting analytic function indicated as solid line. Tables 3 and 4 summarize the quantities measured in the SBF analysis:

Col. 1 – galaxy name and SBF field number,

Col. 2 – pixel size of the SBF field,

Col. 3 – magnitude m_1 of a star yielding 1 ADU per second on the CCD,

Col. 4 – mean galaxy surface brightness within the SBF field in ADU,

Col. 5 – sky brightness in ADU,

Col. 6 – exposure time normalized amplitude P_0 of the best least squares fit at wave number $k = 0$ with fitting error in brackets,

Col. 7 – the scale-free white noise component P_1 in the power spectrum, indicating the ratio of sky to mean galaxy surface brightness within the SBF field.

The contribution from distant background galaxies that are fainter than the cutoff magnitude $m_c = 27 R$ mag to the fluctuation signal P_0 was estimated with the modified Jensen et al. (1998) equation as discussed in Jerjen et al. (2001):

$$P_{\text{BG}} = \frac{p^2}{0.5 \ln 10} 10^{(0.8 \cdot m_1 - 22.99)}$$

where p is the SBF field pixel size in arcsec. The measured signal-to-noise $S/N = (P_0 - P_{\text{BG}}) / (P_1 + P_{\text{BG}})$ (Col. 8) in a SBF field is between 2.3 (F1 for VCC0856) and 13.0 (F3 from VCC1087). The relative contribution of P_{BG} to the signal P_0 (Col. 9) is of the order of three percent.

A rich system of globular clusters (GCs) in the halo of a target galaxy is another source of unwanted surface brightness fluctuations. But as we pointed out elsewhere (Jerjen 2003) the expected number of GCs in bright cluster dwarf ellipticals

is quite low and only a minor issue. The GC frequency (S_N)–luminosity relation for dE,Ns studied in the Fornax and Virgo clusters (Miller et al. 1998) predicts 10–40 GCs for galaxies in the luminosity range covered by our dwarfs. All GCs would be brighter than our cutoff luminosity and excised during the image cleaning process. Therefore, we applied no further correction to the measured SBF power.

5. COLOUR–FLUCTUATION MAGNITUDE DIAGRAMS AND SBF DISTANCES

In the last section we Fourier-analysed the selected SBF fields and measured the fluctuation signals. These signals were converted into a stellar fluctuation magnitude \bar{m}_R using the formula $\bar{m}_R = m_1 - 2.5 \log(P_0 - P_{BG})$. Furthermore, the $(B - R)$ colour for each field was measured from the cleaned B and R master images. Both quantities were corrected for foreground extinction using the IRAS/DIRBE maps of dust IR emission (Schlegel et al. 1998). The results are listed in the Tables 5 and 6.

The power spectrum fitting error is between 2 and 11%. Other sources of minor errors are the PSF normalization ($\sim 2\%$), the shape variation of the stellar PSF over the CCD area (1–2%) and the uncertainty in the photometric calibration (0.03 mag in B , 0.02 mag in R and R_s). If we further adopt a 16% error for the foreground extinction (Schlegel et al. 1998), the formal combined error for a single \bar{m}_R^0 measurement is between 0.05 and 0.14 mag (Col. 3). The error associated with the local colour (Col. 4) has been obtained through the usual error propagation formula from the uncertainties in the sky level determination, the photometry zero points, and Galactic extinction.

The Distance modulus of a program dwarf was then determined by least-squares fitting the set of $[(B - R)_0, \bar{m}_R]$ data to the calibration equations

$$\bar{M}_R = 6.09 \cdot (B - R)_0 - 8.94 \quad (1)$$

for $1.10 < (B - R)_0 < 1.50$

$$\bar{M}_R = 1.89 \cdot [(B - R)_0 - 0.77]^2 - 1.39 \quad (2)$$

for $0.80 < (B - R)_0 < 1.35$.

These linear and parabolic equations were described and discussed at length in Jerjen et al. (2001) and Jerjen (2003). They were deduced from the theoretical $(B - R) - \bar{M}_R$ relation for mainly old, metal-poor stellar populations as predicted by Worthey’s (1994) stellar population synthesis models using the evolutionary isochrones from the Padova library (Bertelli et al. 1994) and an empirical zero point (Jerjen et al. 2001). Fig.5 illustrates the calibration diagram showing model $(B - R)$ and \bar{M}_R values as a function of age, metallicity, and stellar mixture of the underlying stellar population. The solid lines mark the two best-fitting analytical expressions (Eqs.1 and 2).

To obtain the SBF distance of a galaxy with integrated colour redder than $(B - R)_0 \approx 1.35$ (e.g. VCC0929, VCC1010, and VCC1355) is straightforward as the colour–fluctuation magnitude relation is unambiguously represented by eq. 1. However, the task is more difficult for galaxies in the colour regime where both calibration equations are valid ($(B - R)_0 < 1.35$). There, the decision which of the equations to use has to be made based on the observed trend between colour and fluctuation magnitude for the analysed SBF fields. In some cases there is also independent distance information available that renders one of the two solutions more likely than the other. The requirement, or desideratum to cover a

colour range as large as possible has to be borne in mind during the SBF field selection, but sometimes it is impossible to achieve due to the lack of a colour gradient in the dwarf (Barazza et al. 2003). For galaxies like VCC0815, VCC0846, VCC0856, VCC0928, VCC0940, and VCC1422 we found sufficient colour range in the SBF fields. The results are illustrated in Fig. 6 where we show that the colour–fluctuation magnitude diagrams of these dwarfs, with the exception of VCC0928, are best fitted with the linear calibration equation. Judged from the colour–fluctuation magnitude relation over the observed colour range, VCC0928 might fit into either the linear or parabolic branch, but the latter is strongly preferred by the observed velocity of -254 km s^{-1} (cf. Table 1); the linear branch solution would put that galaxy at too large a distance to be compatible with a negative velocity (cf. also §6).

For VCC1104 the colour range covered by the fields is very small, leaving the calibration ambiguous. However, there is a strong constraint put by the TRGB distance of $(m - M)_{TRGB} = 30.98 \pm 0.20 \text{ mag}$ ($15.7 \pm 1.5 \text{ Mpc}$) from the HST observations of Harris et al. (1998). As the tip magnitude of the red giant branch has been shown to be an accurate distance indicator for old and metal-poor stellar populations (e.g. Da Costa & Armandroff 1990; Gratton et al. 1997; Salaris & Cassisi 1998), this result is useful to identify the correct SBF distance. The correlation of \bar{m}_R with the $(B - R)$ colour over the range of galactocentric radii probed by the four subframes in VCC1104 is plotted in Fig. 6. We found a good agreement with the SBF distance modulus $(m - M)_{0,SBF} = 31.15 \pm 0.19 \text{ mag}$ ($17.0 \pm 1.5 \text{ Mpc}$) based on the linear branch while the distance modulus of $(m - M)_{0,SBF} = 30.66 \pm 0.11 \text{ mag}$ from the parabolic branch appears too small and less compatible with the TRGB result given the quoted uncertainties. Therefore, we will adopt a true distance modulus of $(m - M)_{0,SBF} = 31.15 \pm 0.19 \text{ mag}$ for VCC1104 in the following.

The most interesting situation is found for the dwarfs VCC0009 and VCC0490. As shown by their colour–fluctuation magnitude diagram in Fig. 6, the $(B - R, \bar{m}_R)$ data points of each galaxy form two separate groups and the least-squares fitting moves them right onto the two calibration branches. This is the first time that galaxies have been found with data on both branches. Although unusual, this finding is well explained with an age difference between the underlying local stellar populations (see §7). It provides first empirical support for the relative offset of the two theoretical branches. We further note that VCC0490 has two SBF fields (F5 and F6) with similar $(B - R)$ colours but with fluctuation magnitudes that differ by more than 0.4 mag. This apparent discrepancy can only be understood by overlaying the data on the calibration diagram. The case of VCC0490 nicely demonstrates the importance to examine many SBF fields in a galaxy to estimate its distance correctly.

There are four galaxies left, viz. VCC0810, VCC1036, VCC1087, and VCC1261, where the colour range is too small and where no independent distance information as in the case of VCC1104 is available to break the colour branch ambiguity. Their data can be technically fitted either by the linear or the parabolic equation and thus two distances can be inferred for them. We have to leave it to future investigations to find further support for one of the two distances because of lack of independent evidence that could help to resolve the ambiguity. We show in Fig. 7 the best fits of the dwarfs’ colour–fluctuation magnitude diagrams to both calibration equations and quote the two distances in Table 7.

We list in Table 7 the derived SBF distances for all pro-

gram galaxies. The mean 1σ uncertainty in $m-M$, neglecting the calibration ambiguity in those four cases, is 0.17 mag, corresponding to 1.4 Mpc or 8% of the distance. The dominant source of this uncertainty is the error in the $(B-R)$ colour through its strong amplification by the steep colour-fluctuation magnitude relation. This can be compensated only by having a large number of fields for the SBF analysis; the more fields the smaller the resulting error.

The relatively large galaxy sample with SBF distances available allows us to check the quality of our distance calibration. For that purpose we followed Neilsen & Tsvetanov (2000) and tested our data for a possible correlation between the colour and distance modulus. Fig. 4 shows the distance modulus for each galaxy versus the mean color of that galaxy. In the four cases where we have two different distance moduli the data points are interconnected with a vertical line. At a first glance, there seems to be a slight trend in the data for redder galaxies to have shorter distances. But looking more closely, this impression comes mainly from the relatively short distance of the reddest dwarf VCC0929. Do we have reasons to think that VCC0929 is indeed at the near side of the Virgo cluster? VCC0929 is a cluster B object and in projection close to M49 (see Fig. 1). As M49 has a reported distance of 31.0 ± 0.06 mag (Neilsen & Tsvetanov 2000; Tonry et al. 2001) coinciding with the mean distance of the M87 subcluster, i.e. the more nearby of the two major clumps of cluster A (see following section), the short SBF distance of 30.86 ± 0.14 mag for VCC0929 is indeed fully consistent with its location in the cluster. Aside from VCC0929, there is certainly no significant colour trend discernible in Fig. 4.

6. DISTANCE AND STRUCTURE OF THE VIRGO CLUSTER

The individual SBF distances of our dEs range from 14.9 to 21.3 Mpc (Table 7, not counting the ambiguous cases). Clearly, all of these galaxies are members of the Virgo cluster, as was expected from their redshift and morphological appearance. The mean distance modulus, giving each solution of the four ambiguous cases half weight, is $\langle(m-M)_0\rangle = 31.23 \pm 0.06$, or $\langle D \rangle = 17.6 \pm 1$ Mpc. This value is in good accord with the mean Virgo cluster distance derived for giant early-type galaxies from the SBF (Tonry et al. 2001: $m-M = 31.15$, or 17.0 Mpc) and other methods (Neilsen & Tsvetanov 2000, Kelson et al. 2000), as well as for Virgo spiral galaxies (e.g. Graham et al. 1999; but see Saha et al. 1997 and Ekholm et al. 1999 for dissident views). However, as the distance distribution of dEs is broad and highly non-symmetric (see below), a discussion of the cluster mean distance is not very meaningful anymore; the derived mean value is obviously highly sensitive to the inclusion or exclusion of single objects of the sample.

A coarse measure of the distance spread is provided by the standard deviation of dE distance moduli: $\sigma_{\text{obs}} = 0.245$ mag. This has of course to be compared with the mean distance error for a single dwarf which, as quoted above, is $\sigma_{\text{dE}} = 0.169$. The true 1σ distance dispersion of the dwarf ellipticals in the cluster is then

$$\sigma_{\text{cl}} = \sqrt{\sigma_{\text{obs}}^2 - \sigma_{\text{dE}}^2} = 0.177 \text{ mag},$$

or 1.45 Mpc. This corresponds to a total 1σ or 2σ cluster depth of the Virgo cluster of ca. 3 or 6 Mpc, respectively, in accord with the large distance range of 14.9 to 21.3 Mpc found for the dwarfs (cf. Table 7). How does this compare with the tangential cluster dimension? According to Binggeli (1999),

the angular width of the Virgo cluster is $\approx 8^\circ$ (as can also be seen from Fig. 1). Assuming spherical symmetry for the cluster and a mean distance of 17 Mpc, we would then expect a ($\approx 2\sigma$) front-to-back depth of only 2.4 Mpc (0.31 mag). Hence this is evidence that the distribution of Virgo cluster dEs is significantly elongated along the line of sight.

There have been previous reports of a *very* extended (8–20 Mpc), cigar-like distribution of Virgo dEs (Young & Currie 1995). While such a huge depth in the dE population as claimed by Young & Currie has been suspected to be in large part a ‘finger-of-god’ effect due to unaccounted-for observational errors (Binggeli & Jerjen 1998), it is definitively ruled out by our data. On the other hand, the slightly prolate distribution of dEs found here is in excellent agreement with Neilsen & Tsvetanov (2000) and West & Blakeslee (2000) who used the SBF method to determine the distances to giant ellipticals in Virgo. These authors found a similar cluster depth of $\pm(2-3)$ Mpc around M87. Moreover, Arnaboldi et al. (2000) inferred from the luminosity function of intracluster planetary nebulae that the front end of the Virgo cluster is 14%–18% (or $\Delta[m-M] = 0.28$ to 0.36) closer to us than the Virgo core region around M87. The filamentary distribution of Virgo *spirals* has of course been known for a long time. Yasuda et al. (1997) have argued that the distribution of spiral galaxies in the Virgo cluster is best described as an elongated structure along the line-of-sight with a depth of ± 4 Mpc from M87. However, the evidence that such an elongation, if only a milder one, holds for the early type galaxies in the core region as well is unexpected and new, and it is nicely confirmed by our SBF distances of dwarf ellipticals.

But there is more to the distance distribution than just the dispersion. Consider Fig. 8, upper panel, where the distance distribution of our 16 dwarf ellipticals is shown (black histogram, dwarfs with two possible distances being weighted 0.5 at each value). The binned distribution is clearly *bimodal* with a broad major galaxy concentration at $(m-M) = 31.0$ mag (15.8 Mpc), a sharp drop at 31.2 mag (17.4 Mpc) and a narrow secondary peak at 31.33 mag (18.5 Mpc). These structural features are further emphasised when we add the SBF results for 24 giant ellipticals and NGC4486B from Neilsen & Tsvetanov (2000) and Tonry et al. (2001) that are found in our surveyed area (dashed histogram). The 11 ellipticals studied in both references are weighted half at each distance.

To test the bimodality in the distance distribution against the conservative assumption that the entire galaxy sample was drawn from a single Gaussian distribution we used the adaptive Kernel method (Vio et al. 1994) employing a Gaussian kernel. Thereby, distances for giant elliptical galaxies with two independent measurements (Neilsen & Tsvetanov 2000; Tonry et al. 2001) were averaged while distances for dwarf ellipticals with two possible distances were weighted half at each distance. The lower panel in Fig. 8 shows the adaptive kernel distribution of the 41 early-type Virgo galaxies as a solid line. This line was compared with the result from 1000 simulations of 41 randomly distributed objects having the same statistical properties as our sample galaxies, i.e. a mean distance modulus of $(m-M) = 31.15$ and a standard deviation of $\sigma = 0.4$. The mean adaptive kernel distribution and the $\pm 1\sigma$ confidence level lines for these simulations are shown as dashed and dotted lines. The two galaxy concentrations at $(m-M) = 31.00$ mag and 31.33 mag were found to be significant at the 99% (2.5σ) and 89% (1.6σ) level, respectively. It should also be noted that any asymmetric feature in

the true distance distribution tends to be washed out by the errors in the individual distances, i.e. the two peaks will in reality be much narrower.

What could this bimodality mean? It has previously been noted (Binggeli et al. 1993, Binggeli 1999) that the Virgo cluster core (cluster A) shows a pronounced double structure in the projected spatial distribution and in the kinematics of the galaxies. The main, most massive and galaxy-rich clump of cluster A, and of the whole cluster is clearly centered on the supergiant E galaxy M87 (NGC4486). A secondary, less massive and less rich clump, lying about 1° NW to M87, is centered on the giant galaxy M86 (NGC4406). Members of this secondary clump are found to have systematically smaller radial velocities; in particular, all negative velocities tend to be clustered in the M86 region (Binggeli et al. 1993, Binggeli 1999). This has been interpreted in terms of an infall, or subcluster merging scenario. Given the observed kinematic pattern, the M86 subcluster seems to be falling into the main M87 subcluster *from the backside*. In consequence, we might expect to see a bimodality in the distance distribution of Virgo cluster galaxies: a somewhat larger, broader population peaking at a slightly lower-than-average distance, and a smaller, possibly narrower population peaking at a slightly higher-than-average distance, with a separation of 1 to a few Mpc. Not only is this exactly what we see in Fig. 8, very intriguingly the distance modulus of the primary, higher and closer peak, $(m-M)_{\text{peak1}} = 31.00$, roughly coincides with the mean SBF distance modulus for M87 measured by Tonry et al. (2001) and Neilsen & Tsevtanov (2000): $(m-M)_{\text{M87}} = 31.09 \pm 0.08$ mag. Likewise, the position of the secondary peak, $(m-M)_{\text{peak2}} = 31.33$, is perfectly matched by these authors' measurements for the SBF distance of M86: $(M-m)_{\text{M86}} = 31.31 \pm 0.19$ mag.

The bimodal distance distribution of E and dE galaxies in the core of the Virgo cluster is therefore naturally explained by the subcluster merging scenario proposed before (Binggeli et al. 1993, Binggeli 1999). The M87 and M86 subclusters seem to be separated by $\Delta(m-M) \approx 0.3$, or $\Delta D \approx 2.5$ Mpc. With individual distances and radial velocities available for a fairly large sample of Es and dEs, we can now also check whether the galaxies show the expected infall pattern. For this purpose we have plotted in Fig. 9 distance versus heliocentric velocity for all galaxies considered. As the radial velocity dispersion of early-type galaxies in the Virgo cluster is ≈ 600 km s $^{-1}$ (Binggeli et al. 1993), we should not expect to see any streaming motions in the velocity range 0–2000 km s $^{-1}$. However, there is a clear infall signature traced out by the galaxies with negative velocities. As mentioned before, most of these are clustered around M86 (NGC4406), which has a negative velocity itself. They are on average lying on somewhat larger distances than the cluster mean. NGC4419 is an exception, lying in the north of the cluster and being classified as Sa in the VCC. This galaxy likely belongs to a population of surrounding late-type galaxies that have recently fallen into the cluster (see the discussion in VCC). Whether VCC0810, for which two possible distances have been derived (cf. Table 7), is approaching the cluster from behind for the first time or has already fallen through it while still maintaining such a large relative (negative) velocity, is difficult to judge without detailed modeling. The long distance of VCC0810 would in any case appear more likely now, as it is perfectly in accord, like the distances and velocities of M86, VCC00928, VCC0815, and VCC0846, with the virgocentric infall model of Kraan-Korteweg (1986).

7. ESTIMATES OF METALLICITIES AND AGES OF THE DE STELLAR POPULATIONS

The metallicities of dE galaxies are basically unknown. Rakos et al. (2003) estimated a [Fe/H] range from -2 to solar with a mean value around -0.75 . The primary problem in obtaining accurate information about the stellar populations in dEs is because their surface brightnesses are very low, making spectral observations difficult regardless of distance. In the light of those technical obstacles, the much easier to measure field-to-field variation of the SBF magnitude and $(B-R)_0$ colours across a galaxy may serve as a valuable diagnostic tool to get rough metallicities and ages of the unresolved stellar populations.

Given, however, that the age-metallicity degeneracy steadily increases for populations younger than 8 Gyrs (i.e. $[(B-R), \bar{M}_R]$ data points of models move down along the linear branch in Fig. 10), it is essential to base our estimates on age constraints for early-type galaxies as provided by studies using more accurate methods. Stellar absorption-line indices were measured by Caldwell et al. (2003) to disentangle the effects of age and metallicity in a sample of Virgo early-type galaxies. The strong Balmer lines found in these dwarfs were interpreted within the Lick index system as primarily being caused by young age, rather than by low metallicity. Derived galaxy ages ranged from 1–16 Gyrs. This interpretation stands in contrast to Maraston & Thomas (2000, 2001), who showed that a mix of an old metal-rich and an old metal-poor component can produce strong Balmer and metal lines without invoking a young population.

A full investigation of this issue is beyond the scope of this paper but we want to recall instead another result from age-sensitive narrow-band photometry in the modified Strömgren filtersystem by Rakos et al. (2001). These authors derived a mean age of 10 ± 1 Gyrs for a sample of 27 Fornax dwarf ellipticals and thus provide observational support for a lower age limit of ≈ 8 Gyrs for luminous early-type dwarf galaxies in nearby galaxy clusters.

If the main age of the stellar populations in our dEs is 8 Gyrs or older, as we assume in the following, R -band fluctuations and $(B-R)$ colours depend mostly on metallicity as both quantities closely track the temperature of the RGB whose colour is governed by metallicity. This relation allows a direct comparison of the colour range covered by the SBF measurements for an individual dwarf with the corresponding metallicity range.

More quantitatively, we compared each set of observed $[(B-R), \bar{M}_R]$ data points with the predictions of a grid of synthetic stellar populations (Fig. 5): single-burst populations covering the {age=8, 12, 17 Gyr} \times {[Fe/H]= $-1.7, -1.6, \dots, -1.0, -0.5, -0.25, 0$ } parameter space (with [Fe/H] ≥ -1.3 in the case of 17 Gyrs due to model limitations). Taking into account that local dwarf ellipticals show quite a diversity of evolutionary histories with multiple epochs of starformation (e.g. Da Costa 1998; Grebel 1998) we also added a set of composite models where the previously defined single-burst populations were mixed at the 10, 20 and 30% levels (in mass) with a second, intermediate-age generation of 5 Gyrs old stars with solar metallicity. The $(B-R)$ and \bar{M}_R values for each model were computed with Worthey's on-line model interpolation engine³ with a standard Salpeter IMF, using the evolutionary isochrones from the Padova library (Bertelli et al. 1994) and the empirical zero point from Jerjen et al. (2001).

³ http://199.120.161.183:80/~worthey/dial/dial_a_pad.html

The model values are graphically presented in Fig. 5. Single-burst, old, and metal-poor stellar populations have fainter and bluer R -band fluctuations. Their data define the parabolic branch while more metal-rich and/or composite single-burst populations with a minor contribution of intermediate-age stars make up the linear branch. The plot symbols along the linear branch in Fig. 5 covering the 8–17 Gyrs age range indicate that this part of the colour-fluctuation luminosity relation, although degenerated to some level, is primarily a metallicity sequence.

By comparing the location of the SBF data for each dE in Figs. 6 and 7 with Fig. 5 we get rough estimates of the metallicities. Table 8 summarises the results and a brief discussion of each dE is given here:

VCC0009: – appears to be among the purest breed of our sample. The locations of the SBF data on both calibration branches suggest star formation episodes at 17 and 8–12 Gyrs. The metallicity of this major population is $[Fe/H] \approx -1.0$. The data is further consistent with a pollution at the $\approx 10\%$ level with a more metal-rich population of intermediate age stars (5 Gyrs old).

VCC0490: – similar to VCC0009, this dwarf has SBF data points on the parabolic branch and thus appears to have a genuine old stellar population (17 Gyrs) with a metallicity of $[Fe/H] \approx -1.0$ and a second population (8–12 Gyrs) with similar metallicity. Traces of spiral arms found in the R -band image of this galaxy (Jerjen et al. 2001; Barazza et al. 2002) may be evidence for an even younger stellar population. We note that the central part of the dwarf with the spiral structure was not used in the SBF analysis (see §4).

VCC0810: – depending on whether the data is on the parabolic or linear branch (see Fig. 7) we find the following solutions for the stellar population. *Parabolic branch:* main population has an age of 17 Gyrs with $-1.2 < [Fe/H] < -1.0$ and a 20% contribution of a 5 Gyrs old population with solar metallicity. *Linear branch:* 8–12 Gyr old population with metallicity -1.0 .

VCC0815: – is together with VCC0928 the bluest dE in our sample ($B-R=1.15$). Because the SBF data is located on the linear branch it is also the most metal-poor dwarf with a metallicity of $[Fe/H] \approx -1.4$. The main stellar age is between 8 and 12 Gyrs. The presence of a second stellar population remains undetermined.

VCC0846: – The metallicity of the stellar population (8–12 Gyrs) is in the range of $-1.4 < [Fe/H] < -1.0$. The presence of a second stellar population remains undetermined.

VCC0856: – The metallicity of the main stellar population aged between 8 and 12 Gyrs is the range of $-1.4 < [Fe/H] < -1.0$. Caldwell et al. (2003) derived for VCC0856 a much younger age of 3.3–5.2 Gyrs and a 0.6 dex higher metallicity (-0.85 to -0.43). The unique spiral structure observed in this early-type dwarf (Jerjen et al. 2000) could be optical evidence for recent starformation and thus a population of younger stars in this galaxy. We note that the central part of the dwarf with the spiral structure was not used in the SBF analysis (see §4).

VCC0928: – The location of the SBF data on the parabolic branch implies a major population of 90% of 17 Gyrs old stars (metallicity range of $-1.3 < [Fe/H] < -1.0$) with 10% of 5 Gyr old, more metal-rich stars.

VCC0929: – is the most metal-rich dE ($[Fe/H] \approx -0.5$) in our sample as estimated from $(B-R)_0 \sim 1.40$. Caldwell et al. (2003) derive a similar metallicity of $[Fe/H] = -0.52$ and an age of the stellar population of 9.6 Gyrs. This is in good agreement with the lower age limit (8 Gyrs) we assumed for our metallicity estimates.

VCC0940: – The metallicity of the main stellar population is $[Fe/H] \approx -0.7$ with an assumed stellar age of 8–12 Gyrs.

VCC1010: – Metallicity of the 8–12 Gyrs old stellar population is $[Fe/H] \approx -0.5$. A younger population may be present as indicated by the spiral arms (Barazza et al. 2002). We note that the area with the spiral structure was not used in the SBF analysis (see §4). Caldwell et al. (2003) derived a slightly younger age of 5.3–8 Gyrs but with a similar metallicity -0.40 ± 0.34 .

VCC1036: – Depending on whether the data is on the parabolic or linear branch we find the following solutions for the stellar population. *Parabolic branch:* age 17 Gyrs with $[Fe/H] \approx 1.0$, or *linear branch:* $[Fe/H] \approx -0.8$ and a typical stellar age of 8–12 Gyrs. The independent measurements by Caldwell et al. (2003) give an age of 4.6 ± 6.3 Gyrs and a metallicity -0.34 ± 0.39 , favouring our latter results and thus supporting a distance modulus of 31.13 ± 0.17 for this dwarf.

VCC1087: *Parabolic branch:* age 17 Gyrs with $[Fe/H] \approx 1.0$, or *linear branch* $[Fe/H] \approx -0.8$ and stellar age of 8–12 Gyrs.

VCC1104: – The SBF data suggests a metallicity of -1.1 , assuming an age of 8–12 Gyrs.

VCC1261: – Similar to VCC0810 we estimate, depending on which calibration branch is used, *parabolic branch:* age 17 Gyrs with $-1.2 < [Fe/H] < 1.1$ and 20% of a 5 Gyrs old population with solar metallicity, or *linear branch:* a slightly more metal-rich ($[Fe/H] \approx -1.0$), 8–12 Gyrs old population.

VCC1355: – SBF data is located at the intersection of the two branches. Independent of the stellar age, but assuming it to be older than 8 Gyrs, we derive a metallicity of -0.6 .

VCC1422: – Metallicity of the stellar population is the range of $-1.4 < [Fe/H] < -1.0$ with an assumed stellar age between 8–12 Gyrs. Caldwell et al. (2003) derive a metallicity of $[Fe/H] = -0.41 \pm 0.44$ and an age of the stellar population of 4.2 ± 4.5 Gyrs. The presence of a younger population may be indicated by the observed small central edge-on disk (Barazza et al. 2002). But we note that this part of the dwarf was not used in the SBF analysis (see §4).

The broadband colour based metallicities for our Virgo dEs range from $[Fe/H] = -1.4$ to -0.5 . The mean of 0.95 is 0.2 dex more metal-rich than the observed mean for a sample of eight luminous dEs in the Fornax cluster (Jerjen 2003). The latter sample contains none of the metal-rich dEs as VCC0929 and VCC1010 and is centred at a slightly fainter absolute magnitude. We calculated the absolute V magnitudes for the Virgo dEs (Table 8) from their B magnitudes (Barazza et al. 2003), adopting a mean $B-V = 0.72$ colour (Bothun et al. 1989), and employing the newly derived distance moduli. Fig. 10 shows the location of the Virgo dEs in the metallicity- M_V plane. The Virgo dwarfs share a common region with the mentioned Fornax dEs in the interval $-15.7 < M_V < -18.9$. The points scatter nicely around the metallicity-luminosity relation as set out by the low-luminous dEs and dSphs in the Local Group (da Costa 1998) and 10 Fornax dEs (Held & Mould 1994) supporting qualitatively our results. Also included in the figure, for comparison, are the metallicities from Caldwell et al. (2003) for the four common dwarfs VCC0856, VCC0929, VCC1010, and VCC1422. It is not surprising that their data preferentially occupy the region above the metallicity-luminosity relation since higher order Balmer lines were used as age indicators. This leads to younger ages (< 8 Gyrs) and higher metallicities as pointed out by Rakos et al. (2001).

Clearly, our metallicity and age results from the SBF and $(B-R)$ measurements are valid under the assumption that the studied SBF fields in each galaxy represent the dominant stellar populations and that a lower age limit of 8 Gyrs is correct for those systems. Within these constraints, they offer a valuable alternative to obtain rough metallicities and ages of the unresolved stellar populations of early-type dwarf galaxies.

8. CONCLUSIONS

We have presented the first SBF analysis for 16 dwarf elliptical galaxies in the Virgo cluster. Our main results and conclusions are:

1. Following a similar analysis by Jerjen (2003) for For-

- nax cluster dEs, we have shown that the SBF method, by employing a good imager at a 8m-class ground-based telescope such as FORS@VLT, is an efficient tool to determine accurate distances to dwarf ellipticals as far out as 25 Mpc. The semi-empirical calibration of the R -band fluctuation magnitudes is in most cases straightforward to achieve by choosing many fields over the face of the galaxy with differing ($B-R$) colour. The mean uncertainty for an individual galaxy in ($m-M$) is, to be conservative, ≈ 0.2 mag, or roughly 10% in distance.
- The individual SBF distances of the 16 dEs range from 14.9 to 12.3 Mpc, proving Virgo cluster membership for all of them. However, the distance spread is considerable, being roughly twice as large as would be expected if the cluster were spherical symmetric. So even the early-type component of the Virgo cluster is slightly elongated along the line-of-sight, confirming similar findings based on the distribution of giant Es and intracluster PNe.
 - The combined giant + dwarf Virgo early-type SBF distances show a significantly bimodal distribution. There is a broad primary clump of galaxies at $D \approx 16$ Mpc and a narrow secondary clump around 18.5 Mpc. These features can be associated with the two major Virgo core subclusters centered on M87 and M86. The latter, smaller subcluster seems to be falling into the dominating M87 clump from the backside, separated by ca. 2.5 Mpc. A trace of the expected infall pattern is indeed seen in a plot of SBF distance versus heliocentric radial velocity.
 - The large depth and bimodality of the distance distribution of Virgo cluster early types renders a clear-cut

definition of the ‘Virgo cluster mean distance’ difficult. As the M87 subclump, judged from X-ray images, is undoubtedly the most massive structure of the Virgo complex, it is most natural and physically meaningful to identify it with the Virgo cluster proper. In this case the mean distance of the ‘Virgo cluster’ is ≈ 16 Mpc, rather than ≈ 17 Mpc.

- The surface brightness fluctuations of a galaxy also serve as a constraint on its stellar contents. In particular, the model calibration of the observed colour-fluctuation magnitude relation can be used to derive metallicities for the Virgo dEs that agree with narrow-band and spectroscopic measurements. The method works if the dwarfs are at least as old as 8 Gyr, for which there is independent evidence. The SBF metallicities of the present Virgo dEs range from $[\text{Fe}/\text{H}] \approx -1.4$ to -0.5 .
- Given the great potential of the SBF method to determine the distances of Virgo dEs in an efficient way (low costs in terms of telescope time) and with 10% accuracy, it should prove extremely rewarding for our understanding of the 3D structure of that most nearby cluster of galaxies, if this work could be extended and a massive observational campaign be started to get a good fraction of the roughly 800 more dwarf ellipticals in the Virgo cluster left.

We like to thank the ESO staff of the VLT UT1+UT2 for providing excellent quality images in the service observing mode and the anonymous referee for carefully reading the manuscript. The authors are grateful to the *Swiss National Science Foundation* for the financial support of this research project.

REFERENCES

- Arnaboldi, M., Aguerri, J. A. L., Napolitano, N. R., Gerhard, O., Freeman, K. C., Feldmeier, J., Capaccioli, M., Kudritzki, R. P., & Méndez, R. H. 2000, *AJ*, 123, 760
- Barazza, F.D., Binggeli, B., & Jerjen, H. 2002, *A&A*, 391, 823
- Barazza, F.D., Binggeli, B., & Jerjen, H. 2003, *A&A*, 407, 121
- Bertelli, G., Bessan, A., Chiosi, C., Fagotto, F., & Nasi, E. 1994, *A&AS*, 106, 271
- Binggeli, B. 1999, in *The Radio Galaxy Messier 87*, ed. H.-J. Röser, K. Meisenheimer (Berlin: Springer), p.9
- Binggeli, B., & Cameron, L. M. 1991, *A&A*, 252, 27
- Binggeli, B., & Jerjen, H. 1998, *A&A*, 333, 17
- Binggeli, B., Popescu, C. C., & Tammann, G. A. 1993, *A&AS*, 98, 275
- Binggeli, B., Tammann, G. A., & Sandage, A. 1987, *AJ*, 94, 251
- Binggeli, B., Sandage, A., & Tammann, G. A. 1985, *AJ*, 90, 1681 (=VCC)
- Bothun, G. D., Schombert, J. M., & Caldwell, N. 1989, *AJ*, 98, 1542
- Caldwell, N., Rose, J.A., & Concannon, K. D. 2003, *AJ*, 125, 2891
- Conselice, C. J., Gallagher, J. S., & Wyse, R. F. G. 2001, *ApJ*, 559, 791
- Da Costa, G. S. 1998, *Stellar astrophysics for the local group: VIII Canary Islands Winter School of Astrophysics*, eds. A. Aparicio, A. Herrero, and F. Sanchez. Cambridge; New York: Cambridge University Press, p. 351
- Da Costa, G. S., & Armandroff, T.E. 1990, *AJ*, 100, 162
- de Vaucouleurs G. 1961, *ApJS*, 6, 213
- Ekhholm, T., Lanoix, P., Teerikorpi, P., Paturel, G., & Fouqué, P. 1999, *A&A*, 351, 827
- Ferguson, H. C., & Binggeli, B. 1994, *A&ARv*, 6, 67
- Fracas, C., Struble, M. F., & Fanelli, M. N. 1984, *ApJ*, 282, 19
- Gavazzi, G., Boselli, A., Scodreggio, M., Pierini, D., & Belsone, E. 1999, *MNRAS*, 304, 595
- Graham J. A., Ferrarese, L., Freedman, W. L. et al. 1999, *ApJ*, 516, 626
- Gratton R.G., Fusi Pecci, F., Carretta, E. et al. 1997, *ApJ*, 491, 749
- Grebel, E. K. 1998, in *IAU Symp. 192, The Stellar Content of Local Group Galaxies*, ed. P. Whitelock & R. Cannon (San Francisco: ASP), 1
- Hanuschik, R., & Silva, D. 2002, *The Messenger*, No. 108, p. 4
- Harris, W. E., Durrell, P. R., Pierce, M.J., Secker, J. 1998, *Nature*, 395, 45
- Jerjen, H. 2003, *A&A*, 398, 63
- Jerjen, H., Freeman, K. C., & Binggeli, B. 1998, *AJ*, 115, 1840
- Jerjen, H., Freeman, K. C., & Binggeli, B. 2000, *AJ*, 116, 166
- Jerjen, H., Kalnajs, A., & Binggeli, B. 2000, *A&A*, 358, 845
- Jerjen, H., Kalnajs, A., & Binggeli, B. 2001, in *Galaxy Disks and Disk Galaxies*, eds. G. José, S. J. Funes, & Enrico Maria Corsini, ASP Conf. Ser., 230, 239
- Karachentsev, I. D., Karachentseva, V. E., Dolphin, A. E. et al. 2000, 363, 117
- Kelson, D. D., Illingworth, G. D., Tonry, J. L. et al. 2000, *ApJ*, 529, 768
- Kunth, D., & Östlin, G. 2000, *A&ARv*, 10, 1
- Kraan-Korteweg, R. 1986, *A&AS*, 66, 255
- Landolt, A.U. 1992, *AJ*, 104, 340
- Mieske, S., Hilker, M., & Infante, L. 2003, *A&A*, 403, 43
- Maraston, C., & Thomas, D. 2000, *ApJ*, 541, 126
- Maraston, C., & Thomas, D. 2001, *ApSSS*, 277, 295
- Neilsen, E. H. Jr., & Tsvetanov, Z. I. 2000, *ApJ*, 536, 255
- Rakos, K., Schombert, J., Maitzen, H. M., Prugovecki, S., & Odell, A. 2001, *AJ*, 121, 197
- Saha, A., Sandage, A., Labhardt, L., Tammann, G. A., Macchetto, D., & Panagia, N. 1997, *ApJ*, 486, 15
- Saha, A., Sandage, A., Thim, F., Labhardt, L., Tammann, G. A., Christensen, J., Panagia, N., & Macchetto, F. D. 2001, *ApJ*, 551, 973
- Salaris M., & Cassisi S. 1998, *MNRAS*, 298, 166
- Sandage, A., Binggeli, B., & Tammann, G. A. 1985, *AJ*, 90, 1759
- Schlegel, D., Finkbeiner, D., & Davis, M. 1998, *ApJ*, 500, 525
- Tonry, J. L., & Schneider D. P. 1988, *AJ*, 96, 807
- Tonry, J. L., Dressler, A., Blakeslee, J. P., Ajhar, E. A. Fletcher, A. B., Luppino, G. A., Metzger, M. R., & Moore, C. B. 2001, *ApJ*, 546, 681
- Vio, R., Fasani, G., Lazzarin, M., & Lessi, O. 1994, *A&A*, 289, 640

West, M. J., & Blakeslee, J. P. 2000, *ApJ*, 543, L27

Worthey, G., 1994, *ApJS*, 95, 107

Yasuda, N., Fukugita, M., & Okamura, S. 1997, *ApJS*, 108, 417

Young, C.K., & Currie, M. J. 1995, *MNRAS*, 273, 1141

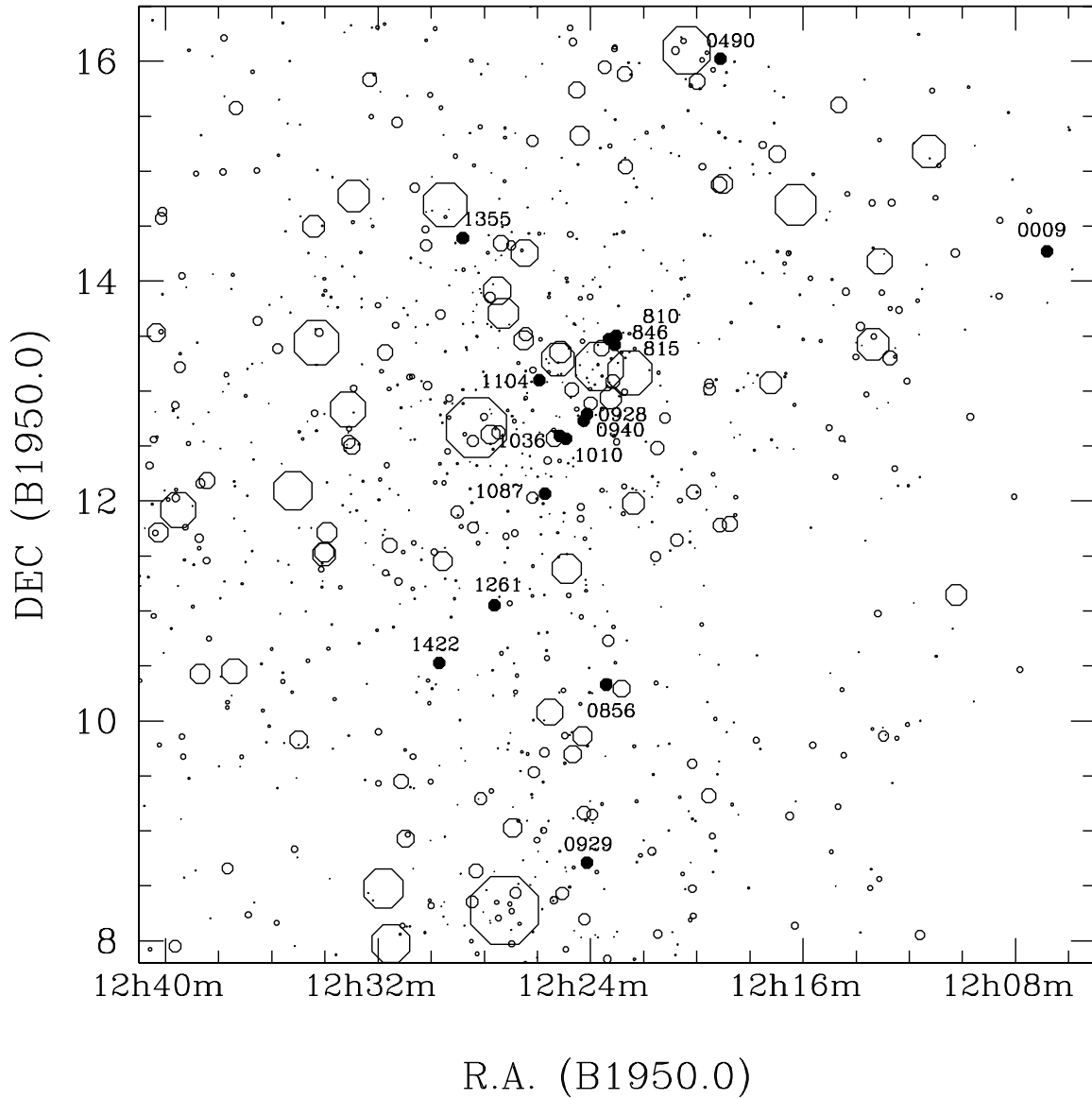


FIG. 1.— A map of all known galaxies in the central region of the Virgo cluster, produced from the Virgo Cluster Catalog. The size of each symbol is proportional to the galaxy luminosity. Filled circles and VCC numbers indicate the locations and names of the dwarf galaxies in our sample. The two most prominent structures known as the M86/M87 subclumps (cluster A) and the M49 cluster (cluster B) are centered on M86 ($12^{\text{h}}23^{\text{m}}39.7^{\text{s}}$, $13^{\circ}13'23''$), M87 ($12^{\text{h}}28^{\text{m}}17.6^{\text{s}}$, $12^{\circ}40'02''$) and M49 ($12^{\text{h}}27^{\text{m}}14.2^{\text{s}}$, $08^{\circ}16'36''$), respectively.

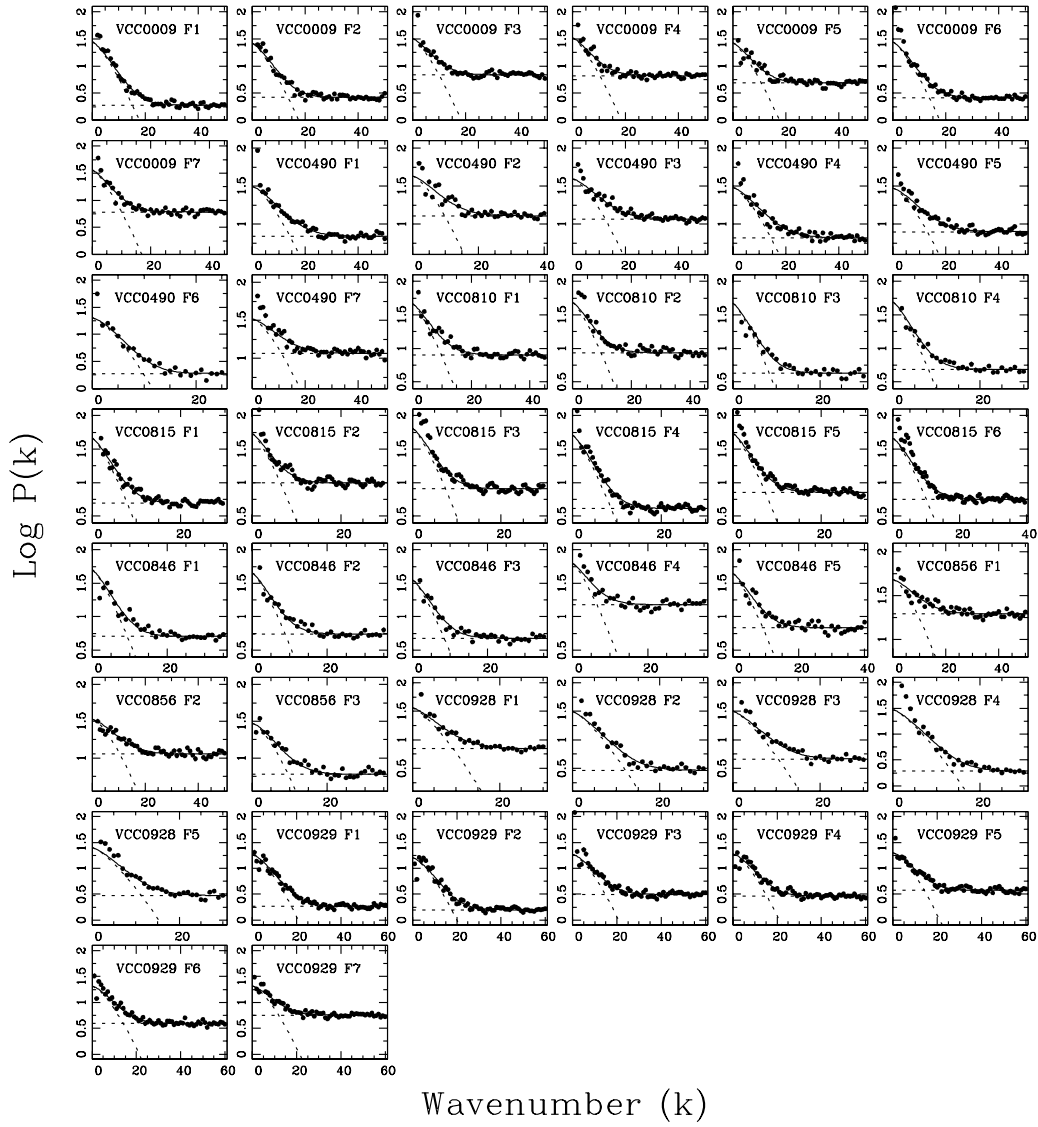


FIG. 2.— Three to seven square fields (subimages) were defined for the SBF analysis distributed over the surface area of each galaxy. We show here the power spectra of the fields analysed in the galaxies VCC0009, VCC0490, VCC0810, VCC0815, VCC0846, VCC0856, VCC0928, and VCC929. The SBF field numbers are indicated after the galaxy name. Corresponding quantities are listed in Table 3. The observations (filled circles) are well fitted by the sum (solid line) of a scaled version of the power spectrum of the stellar PSF and a constant (dashed lines).

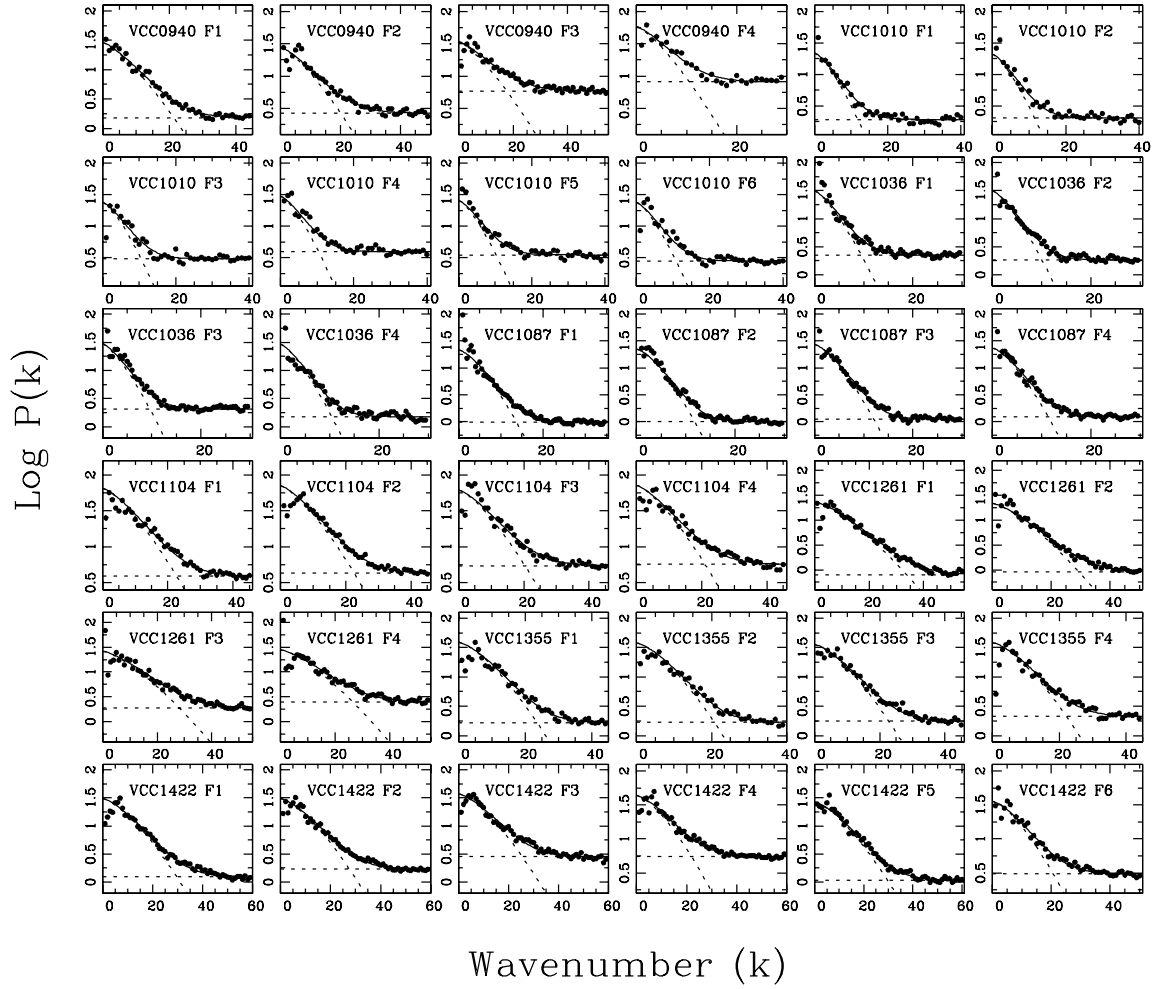


FIG. 3.— The power spectra of all SBF fields analysed in the galaxies VCC0940, VCC1010, VCC1036, VCC1087, VCC1104, VCC1256, VCC1355 and VCC1422. The SBF field numbers are indicated after the galaxy name. Corresponding quantities are listed in Table 4.

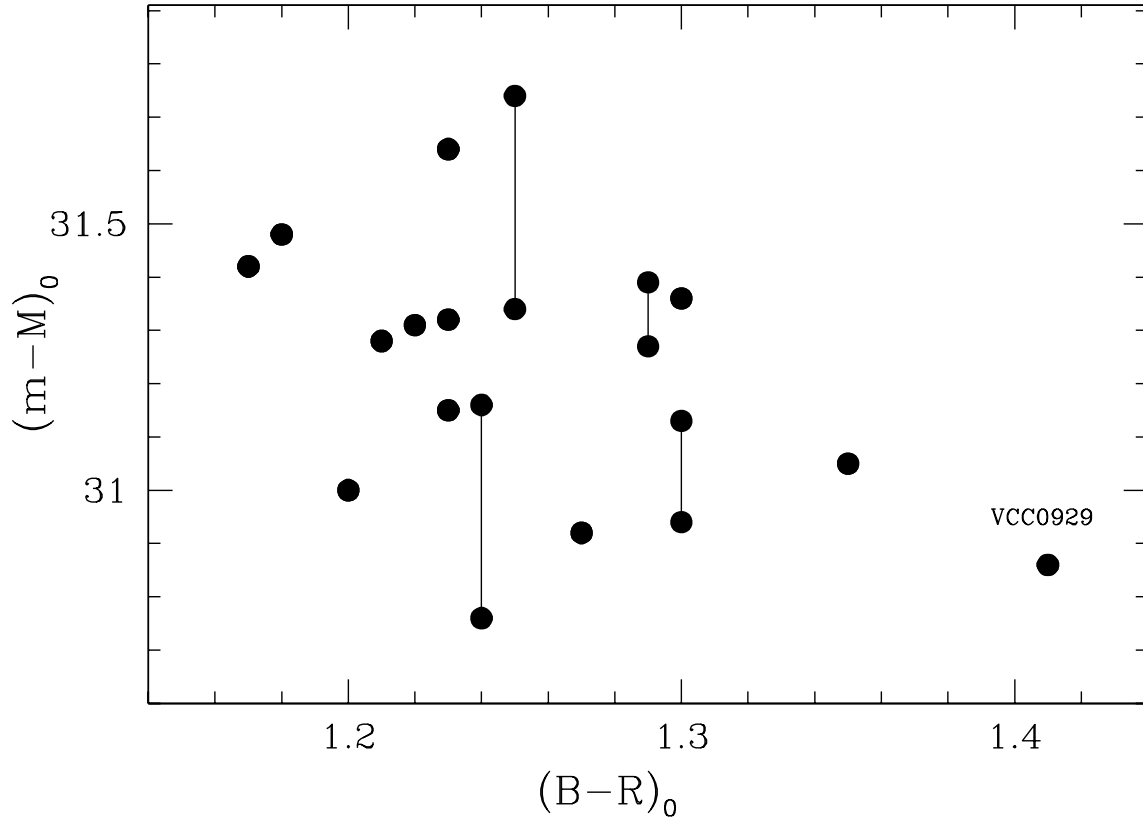


FIG. 4.— A graph showing the mean $(B-R)_0$ colour versus derived distance moduli for the 16 sample dwarf galaxies. Points interconnected by a vertical line are used when the distance measurement was ambiguous. The impression of a slight trend to shorter distances with redder colour is mainly due to the short distance measured for VCC0929. However, being a cluster B member and close to M49, VCC0929 is expected to be slightly more nearby than the cluster in the mean.

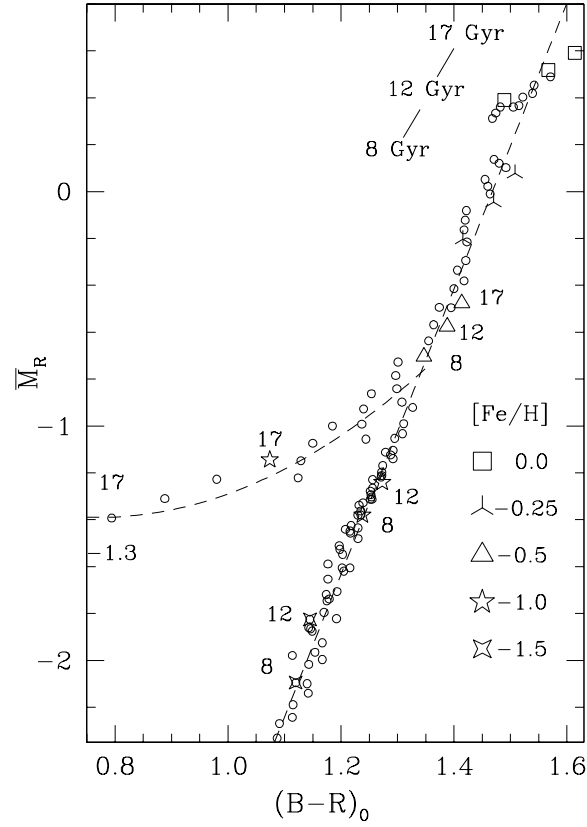


FIG. 5.— SBF calibration diagram showing the Worthey+Padova model predictions of a $(B-R)_0$ colour- R -band fluctuation luminosity relation for a grid of stellar populations (open circles and symbols): a set of single burst populations that covers the $\{\text{age}=8, 12, 17 \text{ Gyr}\} \times \{[\text{Fe}/\text{H}]=-1.7, -1.6, \dots, -1.0, -0.5, -0.25, 0\}$ parameter space (with $[\text{Fe}/\text{H}] \geq -1.3$ in the case of 17 Gyr due to model limitations) and a set of composite populations where the previously defined populations were mixed at the 10, 20 and 30% level (in mass) with a second generation of 5 Gyr old stars with solar metallicity. Also shown are two solid lines representing the best least squares fits to the two branches exhibit by the 116 model points. The parabolic branch stretching from $0.85 < (B-R) < 1.35$ is entirely defined by single-burst, old (> 12 Gyr), metal-poor ($[\text{Fe}/\text{H}] < -0.5$) stellar populations. Slightly younger (8–12 Gyr), more metal-rich single-burst populations and mixed populations with a second burst of star formation fall onto the linear branch from $1.0 < (B-R) < 1.5$. A colour independent offset of 0.13 mag was applied to the original model data to account for the empirical zero point found in Jerjen et al. (2001).

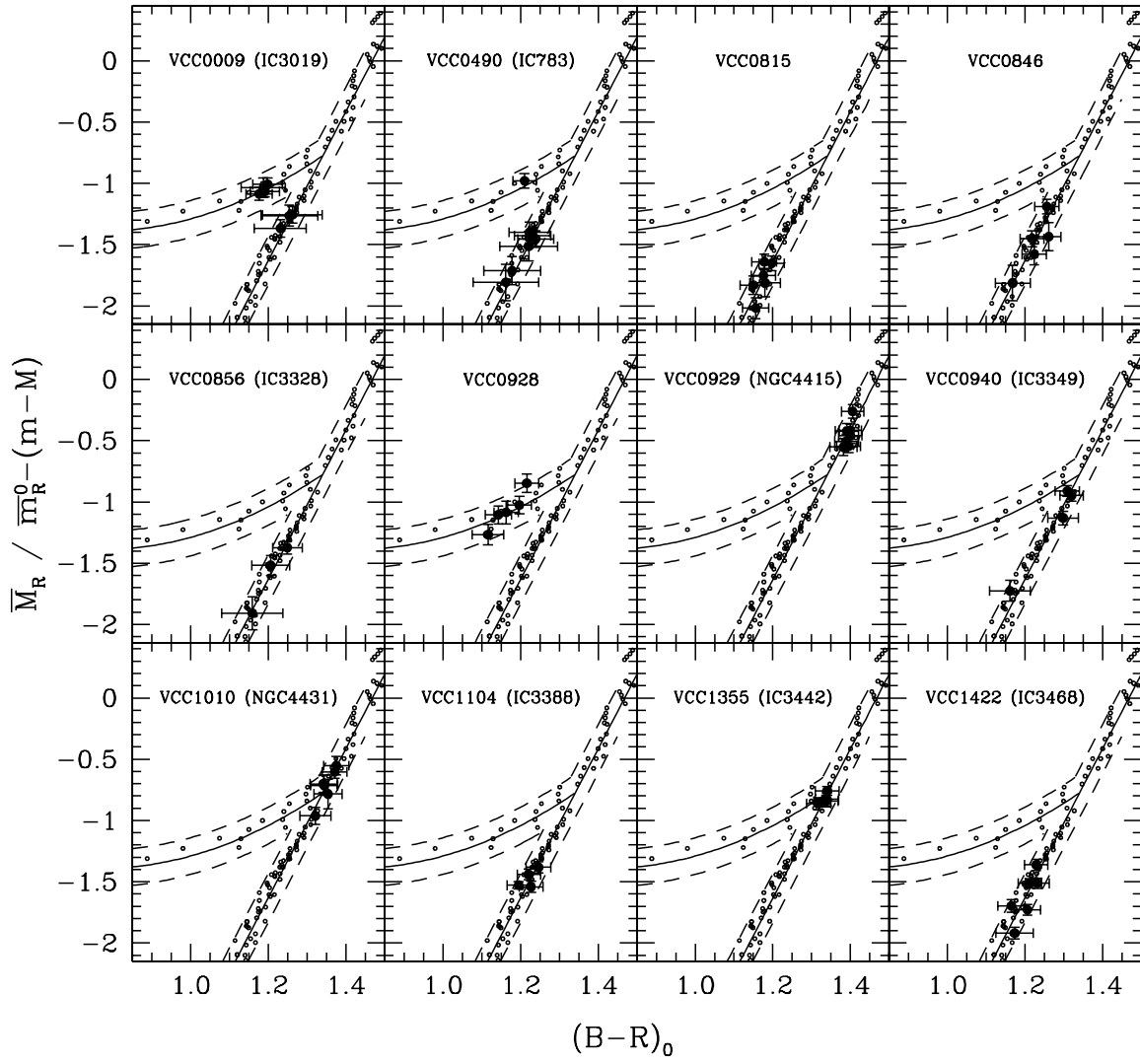


FIG. 6.— The colour-fluctuation magnitude relation for all dwarfs with unambiguous distance. The Fourier analysis of all fields of each sample galaxy yielded a set of apparent fluctuation magnitudes as a function of dereddened local $(B-R)_0$ colour. The data of each galaxy have been shifted along the magnitude axis to get the best fit at one of the loci of absolute fluctuation magnitudes (small circles and solid lines) computed with Worthey's models and using the Padova isochrones with an empirical zero point (see J2003). The derived distance moduli are listed in Table 7. The dashed lines above and below the branches indicate the ± 0.2 mag strip that envelops the intrinsic scatter from different models and the observed scatter in the fluctuation measurements.

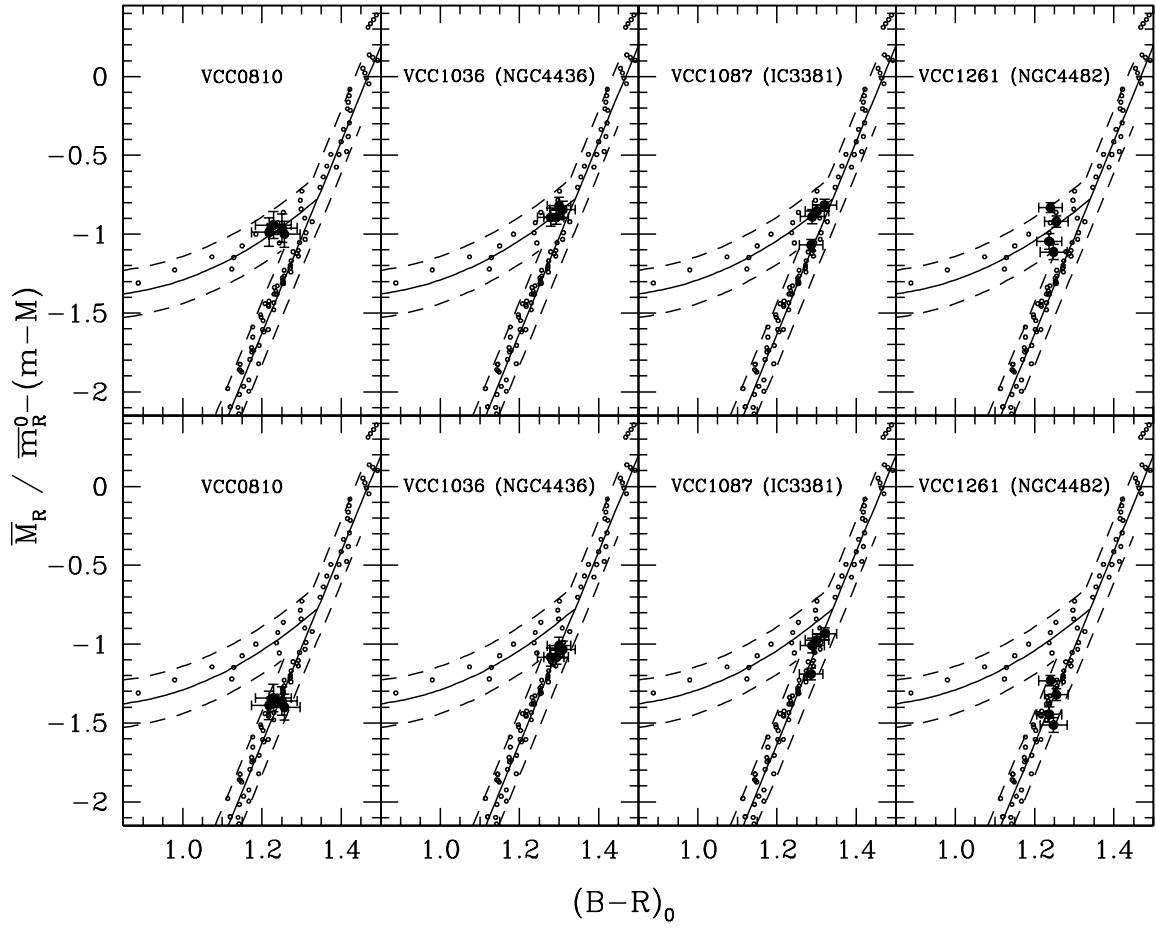


FIG. 7.— The same as Fig.6 but for dwarfs with ambiguous distances. Due to a small color range, the data can be fitted by both calibration equations. The fits producing the shorter distances are shown in the top row while the fits associated to the longer distances are presented in the bottom row (see Table 7).

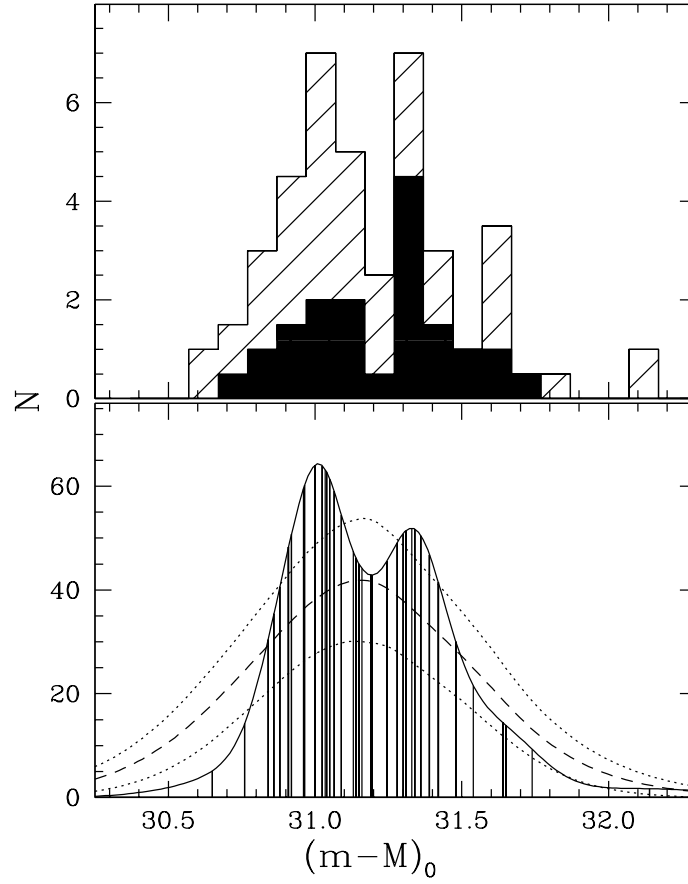


FIG. 8.— (Top panel) Distribution of the SBF distance moduli of 41 early-type dwarf (solid) and giant (dashed) galaxies in the Virgo cluster shown as a histogram binned in intervals of 0.1 mag. Data for the giant ellipticals were taken from Neilsen & Tsevtanov (2000) and Tonry et al. (2001). The binned distribution shows evidence for a bimodality with peaks at $(M-m)_0 \approx 31.0$ and 31.3. (Lower panel) Test of bimodality for the galaxy distribution (solid lines) obtained with the adaptive Kernel method. Mean values (dashed line) and $\pm 1\sigma$ confidence level lines (dotted lines) for 1000 simulations of a Gaussian distribution with the same mean (31.15) and standard deviation (0.4) as the galaxy data are shown. The two concentrations with exact positions at $(M-m)_0 = 31.0$ and 31.33 are significant at the 2.5σ and 1.6σ level, respectively.

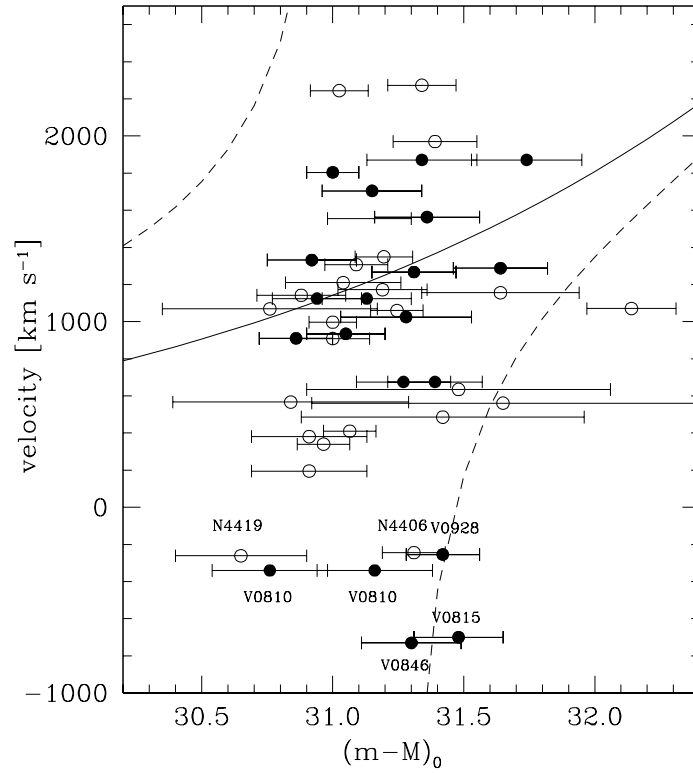


FIG. 9.— Distance as a function of heliocentric velocity. The filled circles represent the dwarfs with SBF distances from this study and the open circle the giant ellipticals with SBF distances from Neilsen & Tsvetanov (2000) and Tonry et al. (2001). The solid line shows the quiet Hubble flow for $H_0 = 70 \text{ km s}^{-1} \text{ Mpc}^{-1}$. A galaxy falling through the cluster center ($D = 17 \text{ Mpc}$) along the line-of-sight would move on one of the dashed lines. These are based on the virgocentric infall model of Kraan-Korteweg (1986) and a Local Group infall velocity of $v_{LG} = 220 \text{ km s}^{-1}$. The galaxies with negative velocities, including NGC4406 (M86) but with the exception of the Sa galaxy NGC4419, follow the expected infall velocity pattern. VCC0810 is shown twice due to two possible distances but its long distance is more likely to be correct (see text).

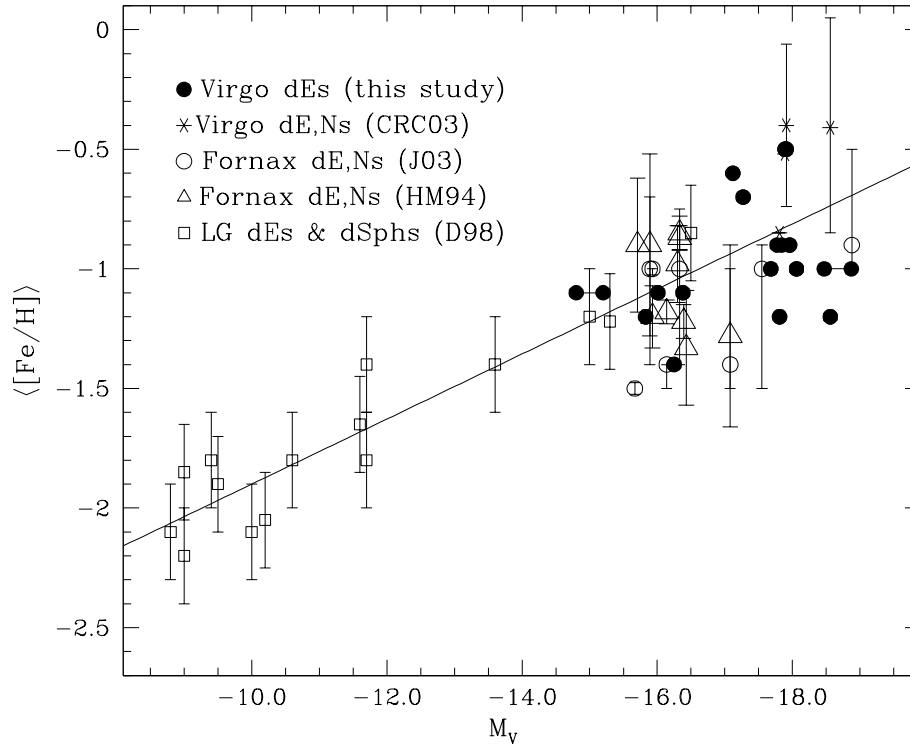


FIG. 10.— The median metallicities plotted as a function of absolute V -band luminosity for our sample Virgo dE,Ns (filled circles). The open circles are metallicities for eight Fornax dEs derived in a similar way from SBF results (Jerjen 2003). The stars, open triangles and squares are the corresponding data for a sample four dEs in the Virgo cluster (Caldwell et al. 2003), 10 Fornax dEs (Held & Mould 1994), and the dEs and dSphs in the Local Group (da Costa 1998). The error bars are taken from the respective reference. The solid line is the best-fitting line at the Local Group data and the brighter Fornax dEs

TABLE 1. BASIC PROPERTIES OF THE OBSERVED EARLY-TYPE DWARF GALAXIES IN THE VIRGO CLUSTER.

VCC Number (1)	Galaxy Name (2)	Morphological Type (3)	R.A. (J2000.0) (4)	Decl. (J2000.0) (5)	Subcluster/Cloud (6)	B_T (mag) (7)	v_{\odot} km s ⁻¹ (8)
0009	IC3019	dE1,N	12h09m22.3s	+13°59′30″	A	14.04	1804
0490	IC0783	dS0(3),N	12h21m38.8s	+15°44′42″	A	13.97	1293
0810	13o42	dE0,N	12h25m33.6s	+13°13′38″	A	16.68	-340
0815	13o47	dE2,N	12h25m37.1s	+13°08′37″	A	15.95	-700
0846	13o48	dE1,N	12h25m50.4s	+13°11′52″	A	16.19	-730
0856	IC3328	dE1,N	12h25m57.9s	+10°03′14″	B	14.19	972
0928	12o42	dE6,N	12h26m39.6s	+12°30′48″	A	16.13	-254 ^a
0929	NGC4415	d:E1,N	12h26m40.9s	+08°26′11″	B	13.69	910
0940	IC3349	dE1,N	12h26m47.1s	+12°27′15″	A	14.81	1563
1010	NGC4431	dS0(5),N	12h27m26.6s	+12°17′27″	A	13.86	913
1036	NGC4436	dE6/dS0(6),N	12h27m41.6s	+12°18′59″	A	13.89	1163
1087	IC3381	dE1,N	12h28m15.1s	+11°47′23″	A	14.15	645
1104	IC3388	dE5,N	12h28m27.9s	+12°49′24″	A	15.49	1704
1261	NGC4482	d:E5,N	12h30m10.4s	+10°46′46″	A	13.59	1850
1355	IC3442	dE2,N	12h31m20.0s	+14°06′54″	A	14.52	1332 ^b
1422	IC3468	E1,N:	12h32m14.2s	+10°15′05″	A	13.80	1372

^aFrom Conselice, Gallagher, & Wyse (2001).

^bthe velocity of 6210 km s⁻¹ quoted for this galaxy in NED is wrong.

TABLE 2. OBSERVING LOG OF THE IMAGING DATA TAKEN IN SERVICE MODE AT THE FORS+VLT.

VCC (1)	Filter (2)	UT Date (3)	Mean Airmass (4)	Exptime (sec) (5)	FWHM (arcsec) (6)	Filter (7)	UT Date (8)	Mean Airmass (9)	Exptime (sec) (10)	FWHM (arcsec) (11)
0009	<i>B</i>	2000-03-28	1.28	3 × 400	0.60	<i>R</i>	1999-07-14	1.55	3 × 400	0.65
0490	<i>B</i>	2000-03-28	1.34	3 × 400	0.70	<i>R</i>	1999-07-10	1.41	3 × 400	0.45
0810	<i>B</i>	2000-05-01	1.41	3 × 600	0.90	<i>R</i>	1999-07-13	1.57	3 × 600	0.60
0815	<i>B</i>	2000-05-01	1.41	3 × 600	0.90	<i>R</i>	1999-07-13	1.57	3 × 600	0.60
0846	<i>B</i>	2000-05-01	1.41	3 × 600	0.90	<i>R</i>	1999-07-13	1.57	3 × 600	0.60
0856	<i>B</i>	2000-03-28	1.29	3 × 400	0.85	<i>R</i>	1999-07-13	1.39	3 × 400	0.55
0928	<i>B</i>	2000-04-01	1.36	3 × 500	0.80	<i>R_s</i>	2000-04-05	1.30	3 × 500	0.60
0929	<i>B</i>	2000-04-05	1.19	3 × 400	0.70	<i>R</i>	1999-07-14	1.47	3 × 400	0.60
0940	<i>B</i>	2000-04-01	1.36	3 × 500	0.80	<i>R_s</i>	2000-04-05	1.30	3 × 500	0.45
1010	<i>B</i>	2000-04-01	1.29	3 × 400	0.70	<i>R_s</i>	2000-04-01	1.25	3 × 400	0.65
1036	<i>B</i>	2000-04-01	1.29	3 × 400	0.65	<i>R_s</i>	2000-04-01	1.25	3 × 400	0.65
1087	<i>B</i>	2000-04-01	1.27	3 × 400	0.65	<i>R_s</i>	2000-04-01	1.24	3 × 400	0.60
1104	<i>B</i>	2000-04-05	1.71	3 × 500	0.55	<i>R_s</i>	2000-04-05	1.51	3 × 600	0.45
1261	<i>B</i>	2000-04-01	1.43	3 × 400	0.85	<i>R_s</i>	2000-04-05	1.23	3 × 400	0.50
1355	<i>B</i>	2000-03-30	1.39	3 × 500	0.90	<i>R_s</i>	2000-04-05	1.40	3 × 500	0.45
1422	<i>B</i>	2000-04-01	1.56	3 × 400	0.75	<i>R_s</i>	2000-04-05	1.21	3 × 400	0.50

TABLE 3. QUANTITIES DERIVED FROM THE SBF ANALYSIS OF VCC0009, VCC0490, VCC0810, VCC0815, VCC0846, VCC0856, VCC0928, AND VCC0929.

Name (1)	size (pixels) (2)	m_1 (mag) (3)	\bar{g} (ADU) (4)	s (ADU) (5)	P_0 (ADU s ⁻¹ pixel ⁻¹) (6)	P_1 (ADU s ⁻¹ pixel ⁻¹) (7)	S/N (8)	P_{BG}/P_0 (9)
VCC0009 F1	100	27.11	1992.9	10326.7	0.070(0.003)	0.005	10.9	0.02
..... F2	100		1393.1		0.065(0.003)	0.007	7.9	0.02
..... F3	100		480.2		0.082(0.004)	0.017	4.3	0.02
..... F4	100		516.7		0.082(0.006)	0.017	4.5	0.02
..... F5	100		681.3		0.067(0.005)	0.012	4.7	0.02
..... F6	100		1412.5		0.069(0.002)	0.006	8.4	0.02
..... F7	100		556.8		0.090(0.005)	0.015	5.3	0.02
VCC0490 F1	100	27.12	952.1	26184.5	0.078(0.003)	0.017	4.1	0.02
..... F2	80		404.8		0.107(0.007)	0.032	3.1	0.01
..... F3	100		486.4		0.098(0.003)	0.029	3.2	0.02
..... F4	100		932.6		0.076(0.003)	0.017	4.1	0.02
..... F5	100		766.3		0.074(0.003)	0.020	3.4	0.02
..... F6	50		3568.1		0.051(0.003)	0.005	7.8	0.03
..... F7	100		498.5		0.082(0.004)	0.029	2.6	0.02
VCC0810 F1	90	27.10	842.3	20052.6	0.078(0.005)	0.013	5.1	0.02
..... F2	60		870.2		0.081(0.006)	0.014	5.0	0.02
..... F3	60		1243.2		0.079(0.006)	0.007	9.0	0.02
..... F4	60		1153.2		0.082(0.006)	0.008	8.3	0.02
VCC0815 F1	60	27.10	942.0	20052.6	0.077(0.003)	0.008	7.7	0.02
..... F2	60		449.8		0.089(0.006)	0.016	4.9	0.02
..... F3	60		653.5		0.108(0.006)	0.013	7.1	0.01
..... F4	60		1277.9		0.085(0.003)	0.007	10.0	0.02
..... F5	60		669.6		0.091(0.003)	0.012	6.6	0.02
..... F6	80		1001.0		0.076(0.003)	0.009	6.9	0.02
VCC0846 F1	70	27.10	1236.3	20052.6	0.084(0.006)	0.008	8.3	0.02
..... F2	70		1107.0		0.075(0.004)	0.009	6.8	0.02
..... F3	70		1246.2		0.059(0.003)	0.008	6.1	0.03
..... F4	70		325.2		0.104(0.007)	0.025	3.8	0.01
..... F5	80		981.9		0.074(0.008)	0.011	5.6	0.02
VCC0856 F1	100	27.12	176.1	10619.7	0.120(0.007)	0.049	2.3	0.01
..... F2	100		357.5		0.084(0.004)	0.028	2.8	0.02
..... F3	70		583.1		0.074(0.002)	0.015	4.4	0.02
VCC0928 F1	60	27.35	503.9	10080.5	0.073(0.005)	0.014	4.3	0.03
..... F2	60		1986.7		0.062(0.006)	0.006	7.3	0.04
..... F3	60		891.6		0.063(0.004)	0.009	5.3	0.04
..... F4	60		2172.5		0.059(0.004)	0.004	9.1	0.04
..... F5	60		2071.7		0.050(0.004)	0.006	5.7	0.05
VCC0929 F1	120	27.12	2830.0	10408.2	0.046(0.002)	0.005	7.2	0.03
..... F2	120		3650.1		0.040(0.002)	0.004	7.0	0.04
..... F3	120		1553.6		0.046(0.003)	0.008	4.7	0.03
..... F4	120		1766.1		0.048(0.003)	0.007	5.2	0.03
..... F5	120		1212.6		0.050(0.003)	0.009	4.4	0.03
..... F6	120		1137.7		0.051(0.002)	0.010	4.4	0.03
..... F7	120		696.5		0.052(0.003)	0.014	3.2	0.03

TABLE 4. QUANTITIES DERIVED FROM THE SBF ANALYSIS OF VCC0940, VCC1010, VCC1036, VCC1087, VCC1104, VCC1261, VCC1355, AND VCC1422.

Name (1)	size (pixels) (2)	m_1 (mag) (3)	\bar{g} (ADU) (4)	s (ADU) (5)	P_0 (ADU s ⁻¹ pixel ⁻¹) (6)	P_1 (ADU s ⁻¹ pixel ⁻¹) (7)	S/N (8)	P_{BG}/P_0 (9)
VCC0940 F1	90	27.35	2663.8	10080.5	0.058(0.002)	0.003	10.2	0.04
..... F2	100		1535.7		0.056(0.002)	0.005	6.9	0.04
..... F3	110		661.8		0.068(0.003)	0.012	4.6	0.04
..... F4	60		342.3		0.116(0.007)	0.016	6.1	0.02
VCC1010 F1	80	27.32	1303.8	8355.3	0.054(0.002)	0.005	7.4	0.04
..... F2	80		1210.8		0.052(0.004)	0.005	6.8	0.04
..... F3	80		876.3		0.060(0.004)	0.008	5.9	0.04
..... F4	80		660.3		0.075(0.004)	0.010	6.0	0.03
..... F5	80		812.0		0.064(0.007)	0.009	5.6	0.04
..... F6	80		947.3		0.059(0.004)	0.007	6.2	0.04
VCC1036 F1	60	27.32	1102.7	8355.3	0.078(0.004)	0.006	9.6	0.03
..... F2	60		1734.3		0.078(0.003)	0.005	11.0	0.03
..... F3	60		1340.8		0.074(0.003)	0.005	9.7	0.03
..... F4	60		2122.0		0.073(0.004)	0.004	11.7	0.03
VCC1087 F1	70	27.31	3198.6	7903.0	0.054(0.002)	0.002	11.1	0.04
..... F2	60		3237.6		0.056(0.002)	0.003	11.4	0.04
..... F3	60		2998.2		0.068(0.002)	0.003	13.0	0.03
..... F4	60		2514.5		0.058(0.002)	0.003	10.4	0.04
VCC1104 F1	90	27.33	2478.4	14213.5	0.108(0.004)	0.006	12.0	0.02
..... F2	90		1933.2		0.117(0.002)	0.007	12.1	0.02
..... F3	90		1516.8		0.102(0.003)	0.009	8.9	0.02
..... F4	90		1913.6		0.118(0.004)	0.009	9.9	0.02
VCC1261 F1	110	27.37	5418.7	7873.2	0.058(0.002)	0.002	12.6	0.04
..... F2	100		4104.7		0.054(0.001)	0.002	10.9	0.05
..... F3	110		1945.4		0.065(0.003)	0.005	8.8	0.04
..... F4	110		983.1		0.069(0.003)	0.006	7.7	0.04
VCC1355 F1	90	27.34	2377.9	10534.8	0.078(0.003)	0.003	13.2	0.03
..... F2	80		2640.1		0.075(0.003)	0.003	12.7	0.03
..... F3	90		2360.9		0.071(0.002)	0.004	11.6	0.03
..... F4	90		1834.7		0.076(0.003)	0.004	11.1	0.03
VCC1422 F1	120	27.38	3695.1	7571.6	0.076(0.002)	0.003	13.0	0.03
..... F2	120		2209.8		0.076(0.003)	0.004	10.8	0.03
..... F3	120		1018.1		0.092(0.003)	0.007	9.4	0.03
..... F4	120		439.2		0.109(0.002)	0.014	6.6	0.02
..... F5	120		3987.8		0.066(0.002)	0.003	12.3	0.04
..... F6	120		876.2		0.089(0.004)	0.008	8.5	0.03

TABLE 5. FLUCTUATION MAGNITUDES AND LOCAL COLOURS FOR EACH SBF FIELD IN VCC0009, VCC0490, VCC0810, VCC0815, VCC0846, VCC0856, VCC0982, AND VCC929. ALL QUANTITIES WERE CORRECTED FOR GALACTIC EXTINCTION.

Name (1)	A_R (mag) (2)	\overline{m}_R^0 (mag) (3)	$(B-R)_0$ (mag) (4)
VCC0009 F1	0.10 ± 0.02	29.91 ± 0.055	1.18 ± 0.03
..... F2		29.99 ± 0.056	1.20 ± 0.04
..... F3		29.74 ± 0.069	1.26 ± 0.08
..... F4		29.74 ± 0.087	1.25 ± 0.07
..... F5		29.96 ± 0.081	1.19 ± 0.06
..... F6		29.93 ± 0.046	1.19 ± 0.04
..... F7		29.63 ± 0.073	1.23 ± 0.07
VCC0490 F1	0.06 ± 0.01	29.86 ± 0.069	1.24 ± 0.05
..... F2		29.50 ± 0.144	1.16 ± 0.08
..... F3		29.60 ± 0.112	1.18 ± 0.07
..... F4		29.88 ± 0.073	1.23 ± 0.05
..... F5		29.91 ± 0.084	1.22 ± 0.05
..... F6		30.33 ± 0.062	1.21 ± 0.03
..... F7		29.80 ± 0.117	1.22 ± 0.07
VCC0810 F1	0.08 ± 0.01	29.82 ± 0.087	1.23 ± 0.04
..... F2		29.77 ± 0.091	1.22 ± 0.04
..... F3		29.80 ± 0.092	1.25 ± 0.04
..... F4		29.76 ± 0.084	1.26 ± 0.04
VCC0815 F1	0.08 ± 0.01	29.83 ± 0.062	1.20 ± 0.03
..... F2		29.67 ± 0.114	1.18 ± 0.04
..... F3		29.46 ± 0.085	1.16 ± 0.03
..... F4		29.73 ± 0.059	1.18 ± 0.03
..... F5		29.65 ± 0.074	1.15 ± 0.03
..... F6		29.84 ± 0.066	1.18 ± 0.03
VCC0846 F1	0.08 ± 0.01	29.74 ± 0.087	1.22 ± 0.03
..... F2		29.87 ± 0.068	1.22 ± 0.03
..... F3		30.13 ± 0.062	1.26 ± 0.03
..... F4		29.51 ± 0.140	1.17 ± 0.05
..... F5		29.88 ± 0.115	1.26 ± 0.03
VCC0856 F1	0.07 ± 0.01	29.37 ± 0.131	1.16 ± 0.08
..... F2		29.76 ± 0.082	1.21 ± 0.05
..... F3		29.91 ± 0.054	1.25 ± 0.04
VCC0928 F1	0.09 ± 0.01	30.14 ± 0.086	1.12 ± 0.04
..... F2		30.33 ± 0.095	1.16 ± 0.03
..... F3		30.30 ± 0.075	1.14 ± 0.03
..... F4		30.38 ± 0.073	1.20 ± 0.03
..... F5		30.56 ± 0.079	1.22 ± 0.03
VCC0929 F1	0.06 ± 0.01	30.44 ± 0.056	1.40 ± 0.03
..... F2		30.60 ± 0.059	1.41 ± 0.03
..... F3		30.44 ± 0.064	1.39 ± 0.03
..... F4		30.40 ± 0.066	1.40 ± 0.03
..... F5		30.36 ± 0.061	1.39 ± 0.03
..... F6		30.31 ± 0.057	1.40 ± 0.03
..... F7		30.31 ± 0.070	1.38 ± 0.04

TABLE 6. FLUCTUATION MAGNITUDES AND LOCAL COLOURS FOR EACH SBF FIELD IN VCC0940, VCC1010, VCC1036, VCC1087, VCC1104, VCC1256, VCC1355 AND VCC1422. ALL QUANTITIES WERE CORRECTED FOR GALACTIC EXTINCTION.

Name (1)	A_R (mag) (2)	\overline{m}_R^0 (mag) (3)	$(B-R)_0$ (mag) (4)
VCC0940 F1	0.08 ± 0.01	30.41 ± 0.051	1.32 ± 0.03
..... F2		30.45 ± 0.047	1.31 ± 0.03
..... F3		30.23 ± 0.058	1.30 ± 0.04
..... F4		29.63 ± 0.086	1.16 ± 0.05
VCC1010 F1	0.08 ± 0.01	30.45 ± 0.056	1.37 ± 0.03
..... F2		30.50 ± 0.077	1.37 ± 0.03
..... F3		30.34 ± 0.083	1.34 ± 0.04
..... F4		30.09 ± 0.071	1.32 ± 0.04
..... F5		30.27 ± 0.122	1.35 ± 0.04
..... F6		30.35 ± 0.073	1.34 ± 0.03
VCC1036 F1	0.07 ± 0.01	30.05 ± 0.060	1.28 ± 0.03
..... F2		30.05 ± 0.049	1.29 ± 0.03
..... F3		30.10 ± 0.056	1.31 ± 0.03
..... F4		30.12 ± 0.058	1.30 ± 0.03
VCC1087 F1	0.07 ± 0.01	30.45 ± 0.042	1.39 ± 0.03
..... F2		30.42 ± 0.044	1.38 ± 0.03
..... F3		30.20 ± 0.042	1.36 ± 0.03
..... F4		30.38 ± 0.050	1.36 ± 0.03
VCC1104 F1	0.06 ± 0.01	29.71 ± 0.048	1.22 ± 0.03
..... F2		29.62 ± 0.036	1.20 ± 0.03
..... F3		29.77 ± 0.048	1.25 ± 0.03
..... F4		29.61 ± 0.048	1.23 ± 0.03
VCC1261 F1	0.08 ± 0.01	30.42 ± 0.041	1.25 ± 0.03
..... F2		30.51 ± 0.038	1.24 ± 0.03
..... F3		30.29 ± 0.053	1.24 ± 0.03
..... F4		30.23 ± 0.051	1.25 ± 0.03
VCC1355 F1	0.09 ± 0.01	30.06 ± 0.054	1.32 ± 0.03
..... F2		30.09 ± 0.057	1.34 ± 0.03
..... F3		30.16 ± 0.041	1.34 ± 0.03
..... F4		30.08 ± 0.050	1.34 ± 0.03
VCC1422 F1	0.09 ± 0.01	30.13 ± 0.043	1.21 ± 0.03
..... F2		30.13 ± 0.047	1.23 ± 0.03
..... F3		29.91 ± 0.048	1.21 ± 0.03
..... F4		29.72 ± 0.051	1.17 ± 0.05
..... F5		30.28 ± 0.049	1.23 ± 0.03
..... F6		29.94 ± 0.054	1.17 ± 0.04

TABLE 7. SBF DISTANCES FOR THE DWARF ELLIPTICALS (AMBIGUOUS CASES LISTED TWICE).

VCC Number (1)	Galaxy Name (2)	$(m-M)_0$ (mag) (3)	D (Mpc) (4)
0009	IC3019	31.00 ± 0.10	15.85 ± 0.80
0490	IC0783	31.31 ± 0.16	18.28 ± 1.46
0810	13o42	30.76 ± 0.13	14.19 ± 0.92
.....	31.16 ± 0.22	17.06 ± 1.88
0815	13o47	31.48 ± 0.17	19.77 ± 1.68
0846	13o48	31.30 ± 0.19	18.20 ± 1.73
0856	IC3328	31.28 ± 0.25	18.03 ± 2.25
0928	12o42	31.42 ± 0.14	19.23 ± 1.34
0929	NGC4415	30.86 ± 0.14	14.86 ± 1.04
0940	IC3349	31.36 ± 0.20	18.71 ± 1.87
1010	NGC4431	31.05 ± 0.15	16.22 ± 1.22
1036	NGC4436	30.94 ± 0.12	15.42 ± 0.93
.....	31.13 ± 0.17	16.83 ± 1.43
1087	IC3381	31.27 ± 0.14	17.95 ± 1.26
.....	31.39 ± 0.18	18.97 ± 1.71
1104	IC3388	31.15 ± 0.19	16.98 ± 1.61
1261	NGC4482	31.34 ± 0.16	18.54 ± 1.48
.....	31.74 ± 0.21	22.28 ± 2.34
1355	IC3442	30.92 ± 0.17	15.28 ± 1.30
1422	IC3468	31.64 ± 0.18	21.28 ± 1.92

TABLE 8. M_V MAGNITUDES AND MEDIAN METALLICITIES DERIVED FROM SBF DATA.

Galaxy (1)	M_V (mag) (2)	[Fe/H] (Median) (3)
VCC0009	-17.68	-1.0
VCC0490	-18.06	-1.0
VCC0810	-15.80/-15.20	-1.1
VCC0815	-16.25	-1.4
VCC0846	-15.83	-1.2
VCC0856	-17.81	-1.2
VCC0928	-16.01	-1.1
VCC0929	-17.62	-0.5
VCC0940	-17.27	-0.7
VCC1010	-17.91	-0.5
VCC1036	-17.77/-17.96	-0.9
VCC1087	-17.84/-17.96	-0.9
VCC1104	-16.38	-1.1
VCC1261	-18.47/-18.87	-1.0
VCC1355	-17.12	-0.6
VCC1422	-18.56	-1.2